The integration of hormonal signaling networks and mobile microRNAs is required for vascular patterning in *Arabidopsis* roots.

Supporting Information

November 28, 2013

Supplementary Figures

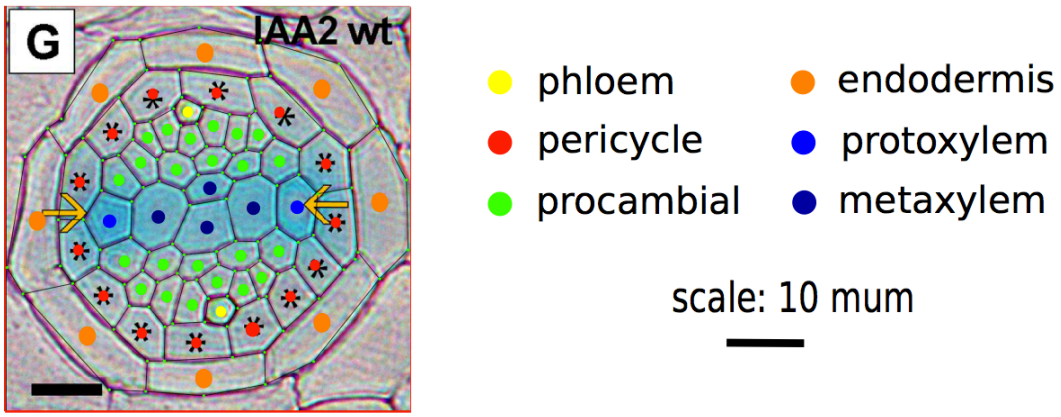

Figure 1: The tissue representation is taken from a cross section through the meristematic region of a primary root. Cell vertices, cell walls and cell types are manually drawn from an image based on *IAA2::GUS* staining. Scale bar = 10 μm.

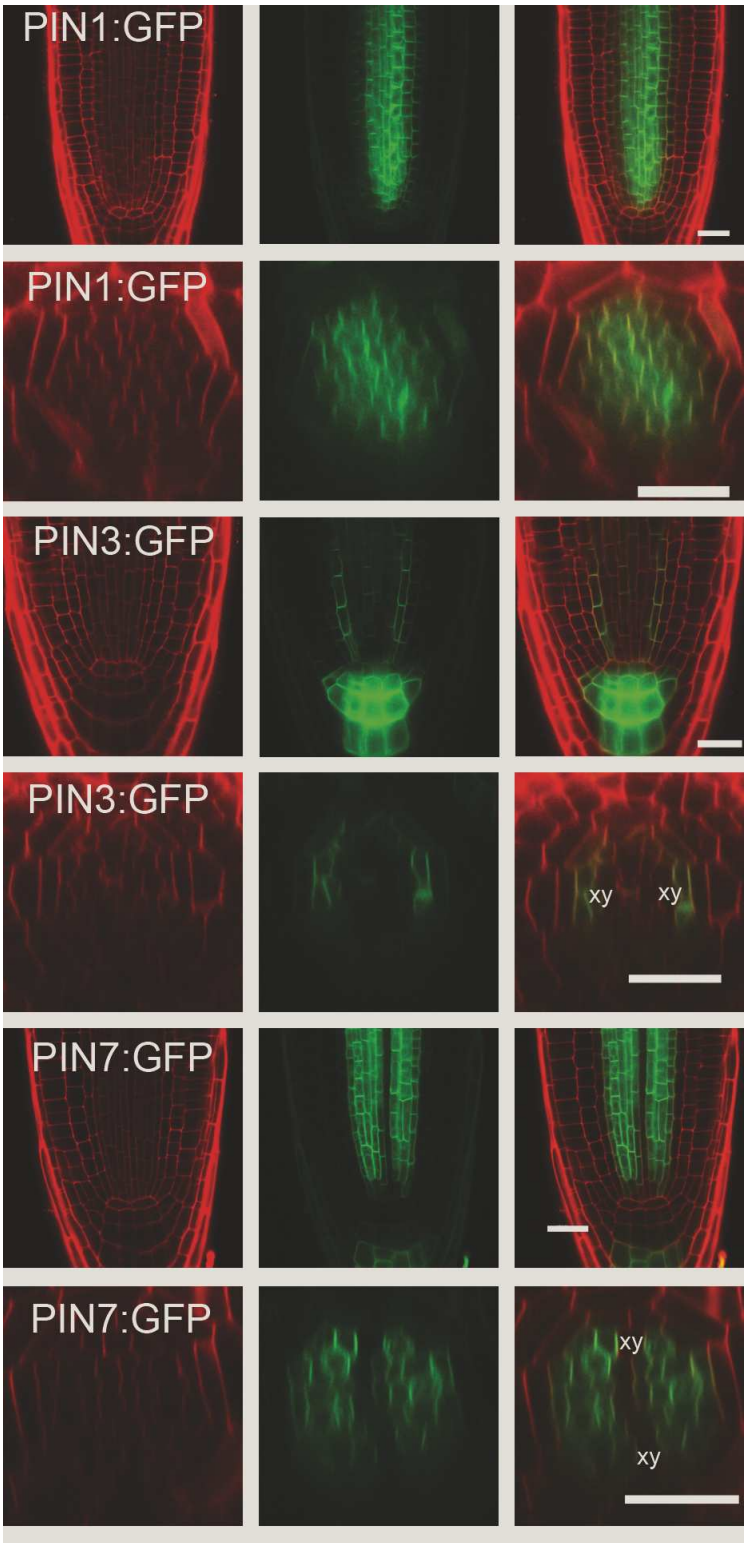

Figure 2: Split channel images of *PIN1::PIN1:GFP*, *PIN3::PIN3:GFP* and *PIN7::PIN7:GFP*. The red channel shows propidium iodide which stains the plasma membrane and the green channel shows GFP. As reported [1] [27] [3] PIN1 is present throughout the stele and PIN7 is present in the procambium, phloem and associated pericycle cells. Whilst there is almost no variation in the patterns of PIN1 and PIN7, some variability exists in the PIN3 pattern and it is sometimes present in a broader domain. However, it is consistently strong in the protoxylem associated pericycle cells. Scale bars = 20 μm.

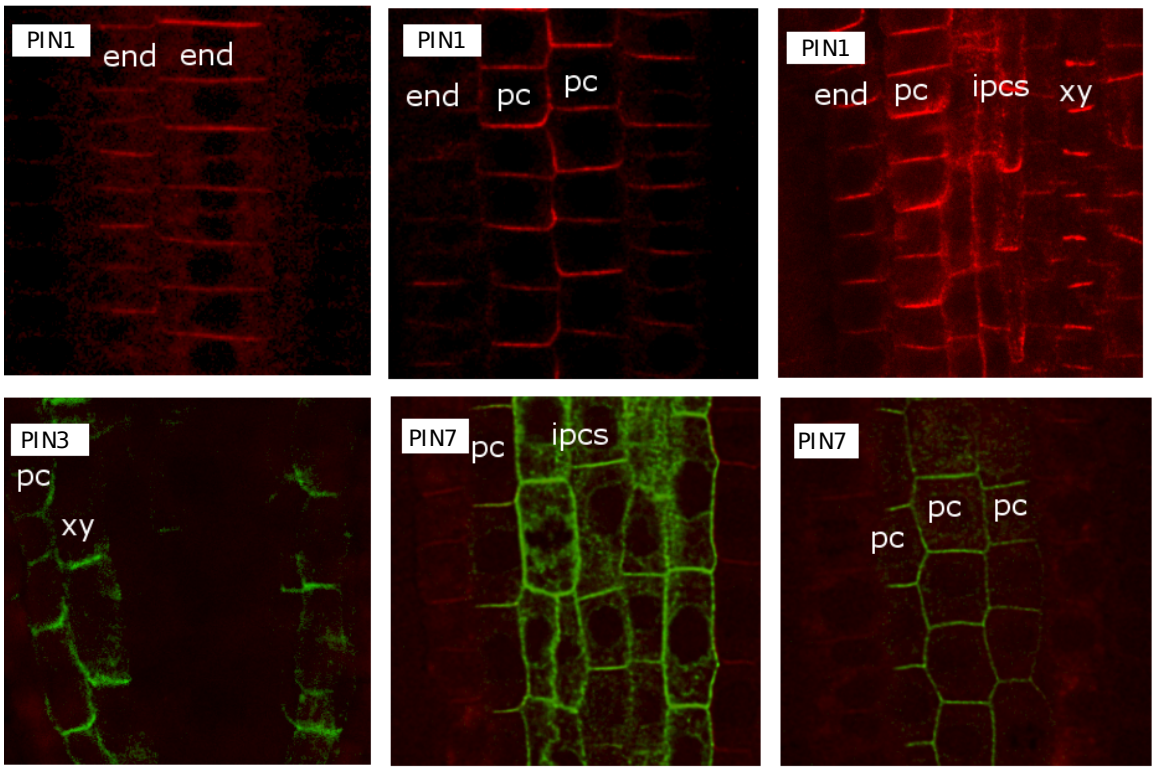

Figure 3: Characterization of PINs with immunolocalization. This allowed us to develop detailed z stacks without the samples bleaching. PIN1 is detected with α-PIN1 antibody, whereas *PIN3::PIN3:GFP* and *PIN7::PIN7:GFP* are detected with α-GFP antibodies. Using this approach we detected PIN1 in the endodermis (labeled end), however it was not localized to any lateral membranes in these cells. We observed PIN1 on the lateral membranes of the pericycle cells (pc). Here it appears to localize to the radial membranes (i.e. directing auxin between the pericycle cells) and the centripetal membranes (i.e. directing auxin into the stele). We did not observe any PIN1 on the centrifugal membranes in the pericycle cells. In the intervening procambial stem cells (ipcs) we observed signal on all lateral membranes. In contrast within the xylem cells (xy) we did not see any lateral localization of PIN1 and the signal was purely localized to the basal membrane. As before, we observed signal in the protoxylem-associated pericycle cells. This appeared to include partial centripetal localization. We also observed some PIN3 signal in the protoxylem. However, this was not accompanied with any observable lateral localization. We observed radial and centripetal localization of PIN7 in the pericycle cells (suggesting that auxin could be directed between these cells and into the vascular cylinder). We observed lateral localization of PIN7 on what appeared to be the radial, centripetal and centrifugal membranes.

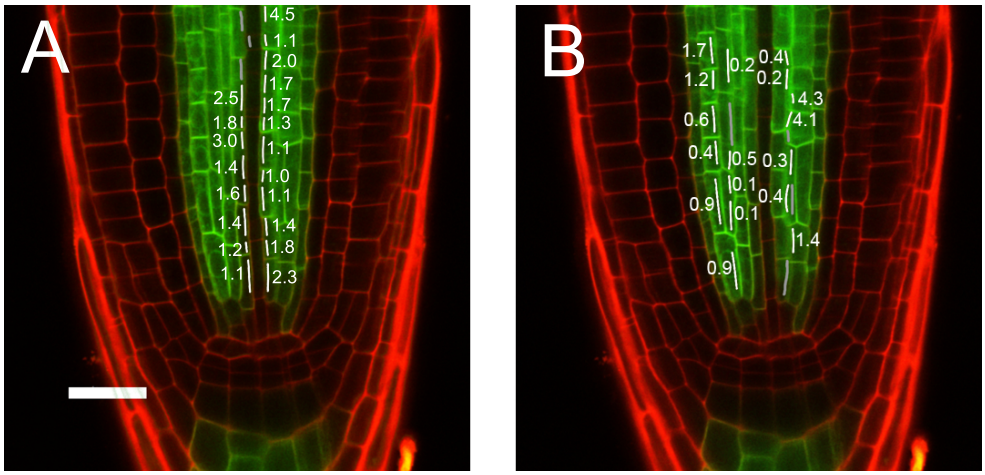

Figure 4: Further analysis of the PIN7 localization by CellSeT [4]. CellSeT segments confocal icaption alignment latexmages and assigns unique identities to each cell and walls between cells. The software then samples the fluorescence offset between the red (propidium iodide stained cell wall) and the green (PIN7:GFP) channels, and produce Gaussian plots of each. It will determine any offset between these Gaussians and report this at sub-pixel accuracy. The offset illustrates the direction in which PINs are localized on the plasma membrane and this information is returned with a confidence value based on the number of offset pixels. Based on this technology, we were able to determine the polarity of PIN7 on the lateral membranes of procambial cells. (A) In the first instance we tested the localization of PIN7 in procambial cells on the walls flanking the xylem axis. As we do not observe any PIN7 within the xylem axis, we expected all of the PIN to be localized on the centrifugal side of this cell wall (i.e. within the procambial cells). We observed this localization 94% of the time (n=46). Furthermore, the 6% of cells where CellSeT reported the PIN to be present in the xylem cells were supported by very low confidence values (0.16 pixels compared with 0.93 pixels). The white lines show which side of the cell wall the GFP signal is predicted and an associated offset value. The gray lines show predictions that are supported with pixel offset values below 0.1.(B) Our confocal images and immunolocalizations suggest that PIN7 was present on all lateral membranes in procambial cells. These were based on observing the confocal images by eye. However, when we see PIN7 associated with a cell wall between two cells expressing *PIN7*, it isn't possible to be sure whether PIN7 is localized on both or just one of the plasma membranes. We reasoned that if PIN7 was present on both cell membranes then it would predict the offset in the cell with the strongest expression of PIN7. However, as PIN7 levels appear to be approximately equal in each of the procambial cells we reasoned that if PIN7 was present in both plasma membranes this would be evident from CellSeT because there would be no clear consensus about which way the PINs would be localized and because the offset values would be relatively low. We observed that in 57% of the cases CellSeT called the offset to be in the centrifugal direction (n=76) and in both the cases where CellSeT predicted either a centrifugal and centripetal offset, these were supported by somewhat lower offset values (0.62 and 0.65 pixels respectively). Taken together these results strongly support our previous observations showing the localization of PIN7 on all lateral membranes in procambial cells.

Figure 5: Documentation of PIN3 localization with CellSeT. The top left image shows the raw confocal image. The software segments the image and identifies and assigns unique numbers to each cell. The user manually assigns cells of interest with GFP expression and selects these cells along with the neighboring cells. Although there is considerable variation, the PIN3 accumulating on the boundary between pericycle cells and their neighbors is predominantly localized on the pericycle-side of the cell wall suggesting that these cells export PIN to their neighbors. We observed this in 70% of pericycle-neighbor boundaries (n=64). An example of a marked up image showing the localization of PIN3 is shown in the left panel. The lower images zoom in on one of the xylem poles. The cell numbered "99" is a protoxylem cell, and the cells numbered "98" and "106" are protoxylem-associated pericycle cells.

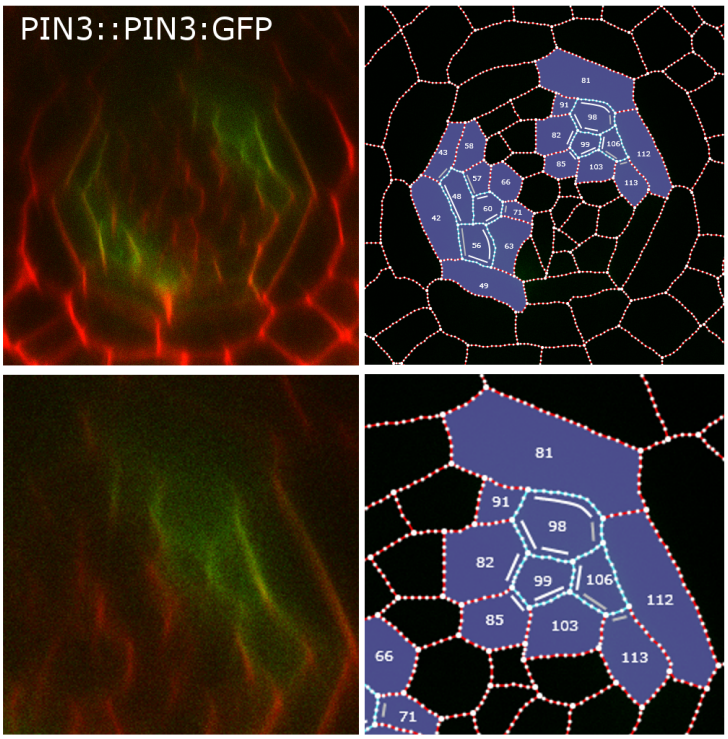

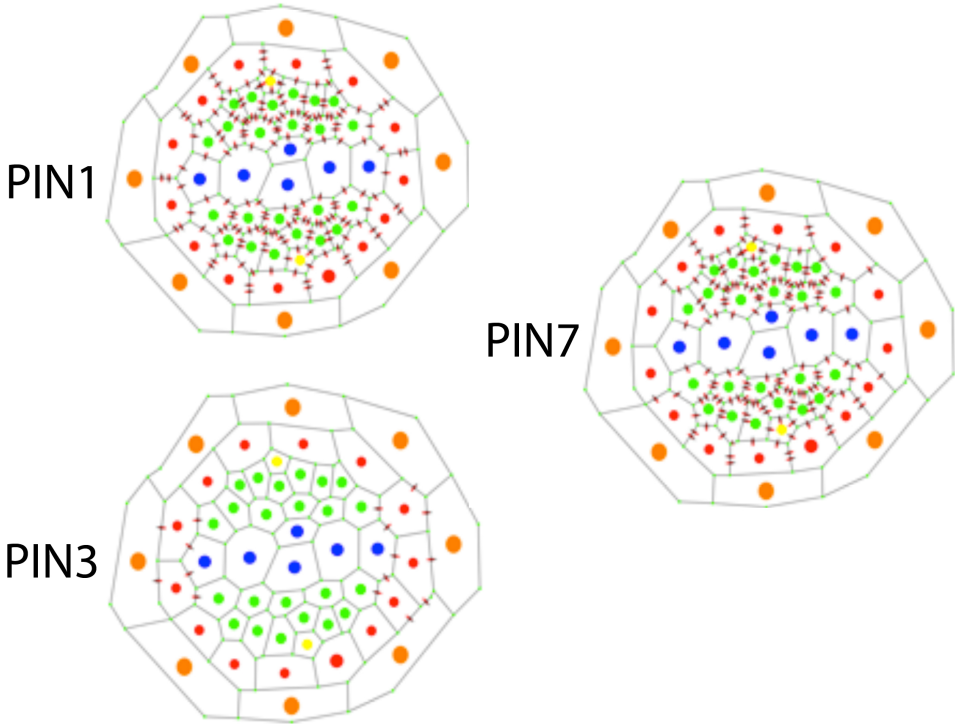

Figure 6: Schematic showing the localization of PINs 1, 3 and 7 used in this study. The cell types are annotated in the same way as FigS1 (phloem = yellow, procambium = green, xylem = blue, pericycle = red and endodermis = orange). The red arrows demonstrate the polarity of the PINs and the direction in which they will transport auxin.

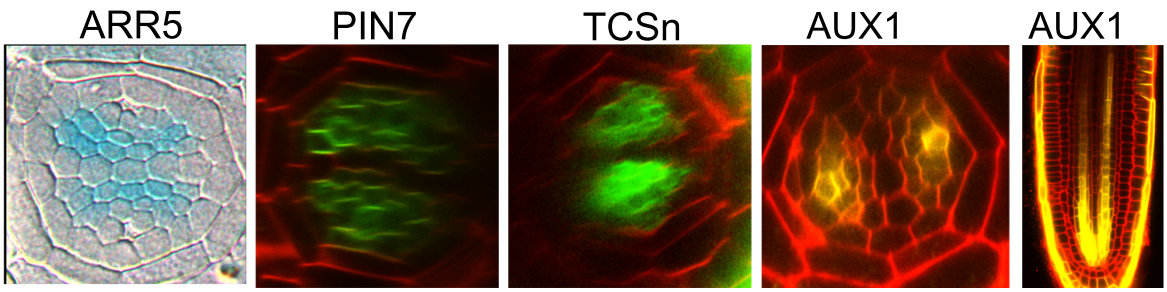

Figure 7: Expression of vascular marker genes. Localization of the three reporters *ARR5*, *PIN7* and *TCSn* confer very similar patterns of cytokinin response in the vascular tissues of the primary root. Localization of *AUX1::AUX1:YFP* shows that AUX1 is localized on the lateral membrane of phloem cells. Although AUX1 signal can be detected in other cells it does not appear to be localized to the lateral membranes in these cells.

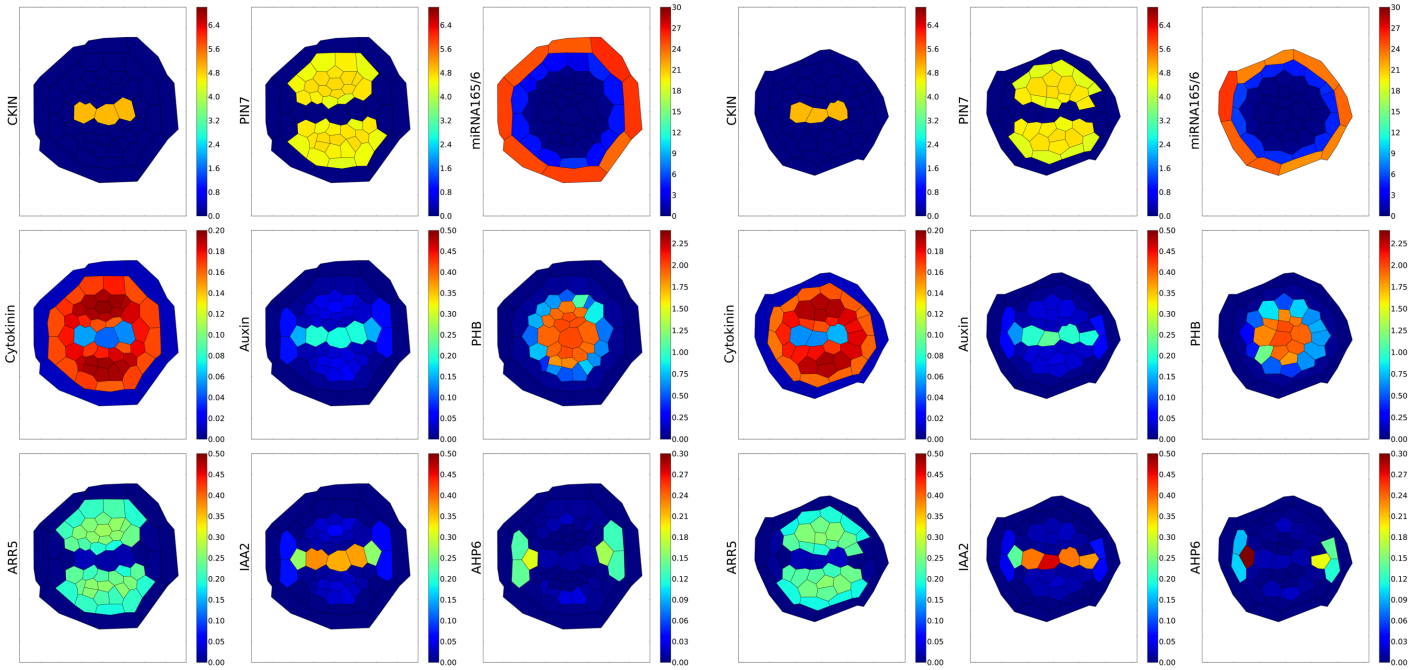

Figure 8: Simulations showing the same model and parameter values as SM7 but using independent root geometries taken at 40 μm above the quiescent centre.

1 Mathematical model applied in Supplementary Movies 1-9

In this section we develop our multicellular mathematical model of vascular patterning in a realistic geometry, as used to generate Supplementary Movies 1-9. Initially, the tissue representation is derived by manually drawing the cell walls and the distribution of auxin efflux transporters PIN1, PIN3 and PIN7 using the open source software Inkscape. Cell wall geometry is reproduced from a digital photograph of a root cross section. The subcellular location of the PINs is based on confocal images (see Supplementary Figures 2 and 3), and in the case of PIN3 and PIN7 has been determined using the CellSeT software [4]. The framework used for the model itself is OpenAlea, an open source software project for plant architecture modeling[5]. Libraries and tools in OpenAlea are primarily based on the use of the high level, object-oriented script language, Python. The .xml format file encoding the cell wall structure plus PIN locations produced by Inkscape is converted into a format compatible for use in OpenAlea using a separate Python script. Once this is done, the sub-cellular interaction network, as summarised in Figure 1 and Supplementary Figure 9, is then coded into ordinary differential equations (ODEs) and embedded in every cell in the realistic tissue structure using the OpenAlea software. The ODE model is derived below, and a table summarizing the species included in the model is reported in Supplementary Table 1.

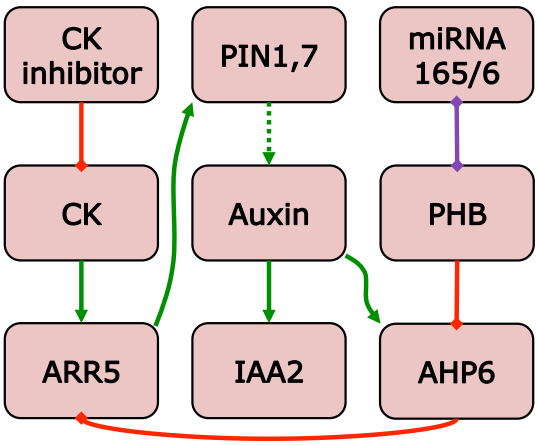

Figure 9: Schematic representation of the network regulating vascular patterning. Green solid arrows indicate gene activation, red solid arrows indicate gene inhibition, the dashed green arrow indicates the transport on auxin mediated by PIN7 and the purple segment represents mutual degradation between miRNA165/166 and *PHB* mRNA.

Species symbol	Species name	Species type
Aux	Auxin	hormone
CK	Cytokinin	hormone
$ARR5_m$	Arabidopsis response regulator 5	mRNA
$ARR5_p$	Arabidopsis response regulator 5	protein
$AHP6_m$	Arabidopsis histidine phosphotransfer 6	mRNA
$AHP6_p$	Arabidopsis histidine phosphotransfer 6	protein
$IAA2_m$	indole-3-acetic acid inducible 2	mRNA
$IAA2_p$	indole-3-acetic acid inducible 2	protein
$PIN1_p$	Arabidopsis thaliana PIN-formed 1	protein
$PIN3_p$	Arabidopsis thaliana PIN-formed 3	protein
$PIN7_m$	Arabidopsis thaliana PIN-formed 7	mRNA
$PIN7_p$	Arabidopsis thaliana PIN-formed 7	protein
PHB_m	Phabulosa	mRNA
PHB_p	Phabulosa	protein
$miRNA165/6$	microRNA 165/6	micro RNA
$CKIN$	Cytokinin inhibitor	unknown

Table 1: *Table summarising the species included in the mathematical model defined by Eqs. (1)-(6).*

Sub-cellular interactions. Our model is based on the following biological hypotheses. All genetic loci are transcribed and translated in every cell and all the species are degraded in every cell except miR165/6 (which is transcribed only in the endodermis) and CKIN (which is transcribed only in the metaxylem. In all other tissues the transcription rates of CKIN and miRNA,p_{miRNA}, p_{CKIN_m}, are set to zero. *PIN1, PIN3* and *PIN7* are located as experimentally observed on the cell walls represented in Supplementary Figure 7 and auxin is actively transported between cells in which at least one of the *PIN* proteins is present.

Based on the above mentioned hypotheses, we model transcription via the following reactions:

$$\emptyset \xrightarrow{p_{AHP6_m} F_{AHP6_m}} \text{AHP6}_m, \qquad \text{AHP6}_m \xrightarrow{d_{AHP6_m}} \emptyset,$$

$$\emptyset \xrightarrow{p_{IAA2_m} F_{IAA2_m}} \text{IAA2}_m, \qquad \text{IAA2}_m \xrightarrow{d_{IAA2_m}} \emptyset,$$

$$\emptyset \xrightarrow{p_{ARR5_m} F_{ARR5_m}} \text{ARR5}_m, \qquad \text{ARR5}_m \xrightarrow{d_{ARR5_m}} \emptyset,$$

$$\emptyset \xrightarrow{p_{PHB_m}} \text{PHB}_m, \qquad \text{PHB}_m \xrightarrow{d_{PHB_m}} \emptyset, .$$

where $p_{AHP6_m}, p_{IAA2_m}, p_{ARR5_m}, p_{PIN7_m}, p_{PHB_m}$ are transcription rates, $d_{AHP6_m}, d_{IAA2_m}, d_{ARR5_m}, d_{PIN7_m}, d_{PHB_m}$

are degradation rates and F_{AHP6_m}, F_{IAA2_m}, F_{ARR5_m} are Hill functional forms given by:

$$\begin{aligned}
F^{(i)}_{AHP6_m}([\text{Aux}]_i, [\text{PHB}_p]_i) &= \frac{([\text{Aux}]_i/\theta_{Aux})^{m_{Aux}}}{1 + ([\text{Aux}]_i/\theta_{Aux})^{m_{Aux}} + ([\text{PHB}_p]_i/\theta_{PHB})^{m_{PHB}}},\\
F^{(i)}_{IAA2_m}([\text{Aux}]_i) &= \frac{([\text{Aux}]_i/\theta_{Aux})^{m_{Aux}}}{1 + ([\text{Aux}]_i/\theta_{Aux})^{m_{Aux}}},\\
F^{(i)}_{ARR5_m}([\text{Aux}]_i, [\text{Ck}]_i) &= \frac{([\text{Ck}]_i/\theta_{Ck})^{m_{Ck}}}{1 + ([\text{Ck}]_i/\theta_{Ck})^{m_{Ck}} + ([\text{AHP6}_p]_i/\theta_{AHP6})^{m_{AHP6}}},
\end{aligned} \tag{1}$$

where i is the cell index, θ_{Aux}, θ_{Ck}, θ_{PHB}, θ_{AHP6} are the binding thresholds of the relevant proteins, m_{Aux}, and m_{Ck}, m_{AHP6} are Hill coefficients. PIN1, PIN3 and PIN7 protein concentrations are divided among the cell walls where these proteins are present (see Supplementary Figure 7). In Supplementary Movies 1-4, their total concentration within each cell containing PINs is fixed to the unitary value, whereas in Supplementary Movies 5-9 only PIN7 is present and its mRNA concentration is governed by the Hill function:

$$F^{(i)}_{PIN7_m}([\text{ARR5}_p]_i) = (\frac{[\text{ARR5}_p]_i/\theta_{ARR5})^{m_{ARR5}}}{1 + ([\text{ARR5}_p]_i/\theta_{ARR5})^{m_{ARR5}}}, \tag{2}$$

where i is the cell index, θ_{ARR5} is $ARR5$ binding threshold and m_{ARR5} its Hill coefficient.

We suppose that *CKIN* mRNA is produced only in the metaxylem via:

$$\emptyset \xrightarrow{p_{CKIN_m}} \text{CKIN}_m, \qquad \text{CKIN}_m \xrightarrow{d_{CKIN_m}} \emptyset,$$

and miRNA165/166 only in the endodermis via:

$$\emptyset \xrightarrow{p_{miRNA}} \text{miRNA165/166}, \qquad \text{miRNA165/166} \xrightarrow{d_{miRNA}} \emptyset$$

where p_{CKIN_m}, d_{CKIN_m}, p_{miRNA}, d_{miRNA} are production and degradation rates. *PHB* mRNA and miRNA165/166 accelerate each other's degradation at rate $d_{miRNA/mRNA}$ as follows [6]:

$$\text{PHB}_m + \text{miRNA165/166} \xrightarrow{d_{miRNA/mRNA}} \emptyset.$$

From the above reactions we obtain the following system of ordinary differential equations:

$$\begin{aligned}
\frac{d[\text{AHP6}_m]_i}{dt} &= p_{AHP6_m} F^{(i)}_{AHP6_m} - d_{AHP6_m}[\text{AHP6}_m]_i,\\
\frac{d[\text{IAA2}_m]_i}{dt} &= p_{IAA2_m} F^{(i)}_{IAA2_m} - d_{IAA2_m}[\text{IAA2}_m]_i,\\
\frac{d[\text{ARR5}_m]_i}{dt} &= p_{ARR5_m} F^{(i)}_{ARR5_m} - d_{ARR5_m}[\text{ARR5}_m]_i,\\
\frac{d[\text{PIN7}_m]_i}{dt} &= p_{PIN7_m} F^{(i)}_{PIN7_m} - d_{PIN7_m}[\text{PIN7}_m]_i,\\
\frac{d[\text{PHB}_m]_i}{dt} &= p_{PHB_m} - d_{PHB_m}[\text{PHB}_m]_i - d_{miRNA/mRNA}[\text{PHB}_m]_i[\text{miRNA165/166}]_i,\\
\frac{d[\text{CKIN}_m]_i}{dt} &= \begin{cases} p_{CKIN_m} - d_{CKIN_m}[\text{CKIN}_m]_i, & \text{if } i \text{ in metaxylem,}\\ 0, & \text{otherwise,} \end{cases}
\end{aligned} \tag{3}$$

Translation of these mRNAs is modelled assuming the following reactions:

$$\begin{aligned}
&\text{AHP6}_m \xrightarrow{p_{AHP6_p}} \text{AHP6}_m + \text{AHP6}_p, && \text{AHP6}_p \xrightarrow{d_{AHP6_p}} \emptyset,\\
&\text{IAA2}_m \xrightarrow{p_{IAA2_p}} \text{IAA2}_m + \text{IAA2}_p, && \text{IAA2}_p \xrightarrow{d_{IAA2_p}} \emptyset,\\
&\text{ARR5}_m \xrightarrow{p_{ARR5_p}} \text{ARR5}_m + \text{ARR5}_p, && \text{ARR5}_p \xrightarrow{d_{ARR5_p}} \emptyset,\\
&\text{PIN7}_m \xrightarrow{p_{PIN7_p}} \text{PIN7}_m + \text{PIN7}_p, && \text{PIN7}_p \xrightarrow{d_{PIN7_p}} \emptyset,\\
&\text{PHB}_m \xrightarrow{p_{PHB_p}} \text{PHB}_m + \text{PHB}_p, && \text{PHB}_p \xrightarrow{d_{PHB_p}} \emptyset,\\
&\text{CKIN}_m \xrightarrow{p_{CKIN_p}} \text{CKIN}_m + \text{CKIN}_p, && \text{CKIN}_p \xrightarrow{d_{CKIN_p}} \emptyset,
\end{aligned}$$

where $p_{AHP6_p}, p_{IAA2_p}, p_{ARR5_p}, p_{PIN7_p}, p_{PHB_p}, p_{CKIN_p}$ are translation rates and $d_{AHP6_p}, d_{IAA2_p}, d_{ARR5_p}, d_{PIN7_p}, d_{PHB_p}, d$ are degradation rates. From these reactions we obtain the following system of ordinary differential equations:

$$\begin{aligned}
\frac{d[\mathrm{AHP6}_p]_i}{dt} &= p_{AHP6_p}[\mathrm{AHP6}_m]_i - d_{AHP6_p}[\mathrm{AHP6}_p]_i,\\
\frac{d[\mathrm{IAA2}_p]_i}{dt} &= p_{IAA2_p}[\mathrm{IAA2}_m]_i - d_{IAA2_p}[\mathrm{IAA2}_p]_i,\\
\frac{d[\mathrm{ARR5}_p]_i}{dt} &= p_{ARR5_p}[\mathrm{ARR5}_m]_i - d_{ARR5_p}[\mathrm{ARR5}_p]_i,\\
\frac{d[\mathrm{PIN7}_p]_i}{dt} &= p_{PIN7_p}[\mathrm{PIN7}_m]_i - d_{PIN7_p}[\mathrm{PIN7}_p]_i,\\
\frac{d[\mathrm{PHB}_p]_i}{dt} &= p_{PHB_p}[\mathrm{PHB}_m]_i - d_{PHB_p}[\mathrm{PHB}_p]_i,\\
\frac{d[\mathrm{CKIN}_p]_i}{dt} &= p_{CKIN_p}[\mathrm{CKIN}_m]_i - d_{CKIN_p}[\mathrm{CKIN}_p]_i.
\end{aligned} \tag{4}$$

Transport and diffusion. The modeling of transport and diffusion is inspired by the auxin transport model developed in [7]. We denote by V_i (μm^3) the volume of cell i and by N_i the set of neighboring cells of cell i. If i and n are two neighboring cells, $S_{i,n}$ (μm^2) denotes the area of the exchange surface, and $[\mathrm{PIN1}_p]_{i,n}$, $[\mathrm{PIN3}_p]_{i,n}$ and$[\mathrm{PIN7}_p]_{i,n}$ are the respective levels of PIN1, PIN3 and PIN7 on the membrane of cell i facing cell n. The sum of each of the membrane bound PINs in a given cell is equal to the total intracellular level of that PIN ($[\mathrm{PIN1}_p]_i$, $[\mathrm{PIN3}_p]_i$ and$[\mathrm{PIN7}_p]_i$), and is distributed between each of the walls with PIN according to the ratio of their surface areas.

We assume auxin, cytokinin and miRNA165/166 to be passively transported between cells, with background permeabilities $P_{Aux}, P_{Ck}, P_{miRNA}$. Auxin is additionally transported actively by PIN carriers with rate T_{Aux}. Assuming that cytokinin biosynthesis is inhibited by CKIN protein, we model such inhibition by the saturating form:

$$F_{Ck}^{(i)}([\mathrm{CKIN}_p]_i) = \frac{1}{1 + ([\mathrm{CKIN}_p]_i/\theta_{CKIN})^{m_{CKIN}}}, \tag{5}$$

where θ_{CKIN} is the binding threshold of the protein CKIN and m_{CKIN} a Hill coefficient. We assume that auxin and cytokinin biosynthesis and degradation occurs in every cell of the root section inside the endodermis and, to account for their transport through the phloem, we enable our model to have different hormone biosynthesis rates in this particular tissue. More precisely, auxin and cytokinin biosynthesis and degradation are governed by the reactions:

$$\emptyset \xrightarrow{p_{Aux}} \mathrm{Aux}, \qquad \mathrm{Aux} \xrightarrow{d_{Aux}} \emptyset,$$
$$\emptyset \xrightarrow{p_{Ck}} \mathrm{Ck}, \qquad \mathrm{Ck} \xrightarrow{d_{Ck}} \emptyset,$$

where p_{Aux}, p_{Ck} are biosynthesis rates and d_{Aux}, d_{Ck} are degradation rates. From the above considerations we obtain the following system of ordinary differential equations:

$$\begin{aligned}
&\frac{d[\mathrm{Aux}]_i}{dt} = p_{Aux} - d_{Aux}[\mathrm{Aux}]_i\\
&- \frac{1}{V_i}\sum_{n\in N_i} S_{i,n}P_{Aux}\Big([\mathrm{Aux}]_i - [\mathrm{Aux}]_n\Big)\\
&- \frac{1}{V_i}\sum_{n\in N_i} S_{i,n}T_{Aux}\Big(([\mathrm{PIN1}_p]_{i,n} + [\mathrm{PIN3}_p]_{i,n} + [\mathrm{PIN7}_p]_{i,n})[\mathrm{Aux}]_i\\
&- ([\mathrm{PIN1}_p]_{n,i} + [\mathrm{PIN3}_p]_{n,i} + [\mathrm{PIN7}_p]_{n,i})[\mathrm{Aux}]_n\Big),\\
&\frac{d[\mathrm{Ck}]_i}{dt} = p_{Ck}F_{Ck} - d_{Ck}[\mathrm{Ck}]_i - \frac{1}{V_i}\sum_{n\in N_i} S_{i,n}P_{Ck}\Big([\mathrm{Ck}]_i - [\mathrm{Ck}]_n\Big),\\
&\frac{d[\mathrm{miRNA165/166}]_i}{dt} = p_{miRNA} - d_{miRNA}[\mathrm{miRNA165/166}]_i\\
&- d_{miRNA/mRNA}[\mathrm{PHB}_m]_i[\mathrm{miRNA165/166}]_i\\
&- \frac{1}{V_i}\sum_{n\in N_i} S_{i,n}P_{miRNA}\Big([\mathrm{miRNA165/166}]_i - [\mathrm{miRNA165/166}]_n\Big),
\end{aligned} \tag{6}$$

where i is the cell index and $p_{miRNA} = 0$ in all cells outside the endodermis.

The experimental evidence suggest that auxin and cytokinin marker genes are absent from the endodermis. To reflect this in the model additional degradation terms are added to the equations for auxin and cytokinin in (6):

$$-\frac{1}{V_i}\sum_{n\in N_i} S_{i,n}P^{end}_{Aux}[\mathrm{Aux}]_i,$$

$$-\frac{1}{V_i}\sum_{n\in N_i} S_{i,n}P^{end}_{Ck}[\mathrm{Ck}]_i,$$

for i in the endodermis. These terms also account for loss of auxin and cytokinin to the outer root tissues not included in the tissue geometry and, in the case of auxin, from top-down transport in the primary root. To keep auxin and cytokinin at a low level in the endodermis we set $P^{end}_{Aux} = 20.0 \cdot \mu m \cdot \mu M^{-1} \cdot s^{-1}$ and $P^{end}_{Ck} = 100.0 \cdot \mu m \cdot \mu M^{-1} \cdot s^{-1}$.

In Supplementary Movie 9 we include the influx carrier AUX1 and we model auxin transport as follows:

$$\frac{d[\mathrm{Aux}]_i}{dt} = p_{Aux} - d_{Aux}[\mathrm{Aux}]_i - \frac{1}{V_i}\sum_{n\in N_i} S_{i,n}P_{Aux}\Big([\mathrm{Aux}]_i - [\mathrm{Aux}]_n\Big)$$
$$-\frac{1}{V_i}\sum_{n\in N_i} S_{i,n}T_{Aux}\Big([\mathrm{PIN7}_p]_{i,n}[\mathrm{Aux}]_i - [\mathrm{PIN7}_p]_{n,i}[\mathrm{Aux}]_n\Big)$$
$$-\frac{1}{V_i}\sum_{n\in N_i} S_{i,n}T_{AUX1}\Big([\mathrm{AUX1}]_{n,i}[\mathrm{Aux}]_n - [\mathrm{AUX1}]_{i,n}[\mathrm{Aux}]_i\Big),$$

where T_{AUX1} is the influx rate due to AUX1 expression. AUX1 is localised on all the membranes of the phloem cells and is constantly expressed in the phloem, its unitary concentration being proportionally divided on the cell walls.

Parameters. As in other mathematical analyses of signaling networks, only partial information is known about the parameter values of the model [8], [9]. As in [8], the parameter values have been specified as follows. The parameters relating to auxin transport efficiency (T_{Aux}) and auxin background permeability (P_{Aux}) have been analyzed in [10], [11] and we use the same values for those parameters (see Supplementary Table 2).

Parameter	Description	Value
T_{Aux}	Transport efficiency of PIN proteins	$20.0 \cdot \mu m \cdot \mu M^{-1} \cdot s^{-1}$
P_{Aux}	Auxin background permeability	$1.0 \cdot \mu m \cdot s^{-1}$
P_{Ck}	Cytokinin background permeability	$10.0 \cdot \mu m \cdot s^{-1}$
P_{miRNA}	miRNA background permeability	$1.5 \cdot \mu m \cdot s^{-1}$
p_{Aux}	Auxin biosynthesis rate	$0.06 \cdot \mu M \cdot s^{-1}$
p_{Ck}	Cytokinin biosynthesis rate	$2.0 \cdot \mu M \cdot s^{-1}$
p_{CKIN_p}	CKIN protein translation rate	$1.0 \cdot s^{-1}$
p_{AHP6_p}	AHP6 protein translation rate	$1.0 \cdot s^{-1}$
p_{IAA2_p}	IAA2 protein translation rate	$10.0 \cdot s^{-1}$
p_{ARR5_p}	ARR5 protein translation rate	$10.0 \cdot s^{-1}$
p_{PIN7_p}	PIN7 protein translation rate	$5.0 \cdot s^{-1}$
p_{PHB_p}	PHB protein translation rate	$1.0 \cdot s^{-1}$
d_{Aux}	Auxin degradation rate	$1.0 \cdot s^{-1}$
d_{Ck}	Cytokinin degradation rate	$10.0 \cdot s^{-1}$
d_{CKIN_p}	CKIN protein degradation rate	$1.0 \cdot s^{-1}$
d_{AHP6_p}	AHP6 protein degradation rate	$1.0 \cdot s^{-1}$
d_{IAA2_p}	IAA2 protein degradation rate	$10.0 \cdot s^{-1}$
d_{ARR5_p}	ARR5 protein degradation rate	$10.0 \cdot s^{-1}$
d_{PIN7_p}	PIN7 protein degradation rate	$1.0 \cdot s^{-1}$
d_{PHB_p}	PHB protein degradation rate	$1.0 \cdot s^{-1}$

Table 2: *Default values of the parameters regulating translation and cell-to-cell communication.*

Parameter	Description	Value
p_{miRNA}	miRNA165/166 transcription rate	$32.5 \cdot \mu M \cdot s^{-1}$
p_{CKIN_m}	*CKIN mRNA* transcription rate	$5.0 \cdot \mu M \cdot s^{-1}$
p_{AHP6_m}	*AHP6* mRNA transcription rate	$2.0 \cdot \mu M \cdot s^{-1}$
p_{IAA2_m}	*IAA2* mRNA transcription rate	$10.0 \cdot \mu M \cdot s^{-1}$
p_{ARR5_m}	*ARR5*mRNA transcription rate	$20.0 \cdot \mu M \cdot s^{-1}$
p_{PIN7_m}	*PIN7* mRNA transcription rate	$1.0 \cdot \mu M \cdot s^{-1}$
p_{PHB_m}	*PHB* mRNA transcription rate	$2.0 \cdot \mu M \cdot s^{-1}$
d_{miRNA}	miRNA165/166 degradation rate	$1.0 \cdot s^{-1}$
d_{CKIN_m}	*CKIN mRNA* degradation rate	$1.0 \cdot s^{-1}$
d_{AHP6_m}	*AHP6* mRNA degradation rate	$1.0 \cdot s^{-1}$
d_{IAA2_m}	*IAA2* mRNA degradation rate	$10.0 \cdot s^{-1}$
d_{ARR5_m}	*ARR5* mRNA degradation rate	$10.0 \cdot s^{-1}$
d_{PIN7_m}	*PIN7* mRNA degradation rate	$1.0 \cdot s^{-1}$
d_{PHB_m}	*PHB* mRNA degradation rate	$1.0 \cdot s^{-1}$
$d_{miRNA/mRNA}$	miRNA165/166 - PHB mRNA mutual degradation rate	$10.0 \cdot \mu M^{-1} \cdot s^{-1}$
θ_{Aux}	Auxin binding threshold	$0.25 \cdot \mu M$
θ_{CKIN}	CKIN binding threshold	$0.05 \cdot \mu M$
θ_{AHP6}	AHP6 binding threshold	$0.04 \cdot \mu M$
θ_{PHB}	PHB binding threshold	$0.4 \cdot \mu M$
θ_{Ck}	Cytokinin binding threshold	$0.5 \cdot \mu M$
θ_{ARR5}	ARR5 binding threshold	$0.1 \cdot \mu M$
m_{Aux}	auxin Hill coefficient	2.0
m_{Ck}	cytokinin Hill coefficient	2.0
m_{AHP6}	AHP6 Hill coefficient	3.0
m_{PHB}	PHB Hill coefficient	3.0
m_{ARR5}	ARR5 Hill coefficient	3.0
m_{CKIN}	CKIN Hill coefficient	5.0

Table 3: *Default values of the parameters regulating transcription. The Hill coefficients have been set greater than one to reflect a non-linear response of genes to activators and repressors. Where known, these have been chosen to reflect the presence of multiple binding sites within a promoter or the number of genes required for a given response. For example, both* A*HP6 and* I*AA2 contain multiple Auxin Response Elements (AuxREs).*

Following [10], we assume that the ratio between rates of active and passive transport to be 1/20. The other parameters are unknown: initially, as proposed in [8], all unknown parameters were set to be unity of their particular unit; subsequently, some have been modified in the light of experimental observations. We explored a range of values for the production and degradation of *PHB* mRNA and miR, and selected realistic values from this range that reproduced the patterns observed in [12]. We subsequently examined the effect that altering these values had (see section 2) and found that quite significant changes were required in order to disrupt the gradient of *PHB*. Due to the partial arbitrariness of the parameter choice, and to test the robustness of the model results, in the following sections we develop local and global sensitivity analyses of our signaling network model in single cells, taken from different tissues, and we analyze the effects of parameter perturbations in the two-dimensional geometry. The default parameter values and units used in the multicellular model are reported in Supplementary Tables 2, 3. Variations around these values have been applied to produce Supplementary Movies 1-7 and are reported in the legends of the Supplementary Movies. With this choice of parameters the model evolves to a stable pattern in approximately 15 seconds simulated time (see Supplementary Movies 1-7). A typical simulation result is presented in Supplementary Movie 6.

2 Exploration of parameter space in *PHB* - miRNA165/6 sub model

The spatial distribution of PHB protein is modified in the model solely via the interaction and mutual degradation of miRNA and *PHB* mRNA. Because of this the equations for both in (3) and (6) may be considered as a separate sub-model defining the spatial expression of *PHB* mRNA. Figure 10(a) shows the steady state distribution of *PHB* mRNA using the default parameter values given in Table 3. The robustness of model *PHB* expression pattern to parameter changes was tested by considering the mean mRNA values in five concentric cell layers as shown in Figure 10(b). These were then plotted relative to the peak *PHB* expression in the central layer (L1) for a variety of parameter values. The distribution for the default parameter set is shown in figure 10(c). *PHB* mRNA distributions for variations in each of the default parameter values for $d_{miRNA/mRNA}$, p_{PHB_m}, d_{PHB_m}, P_{miRNA}, d_{miRNA} and p_{miRNA} are shown in Figure 11.

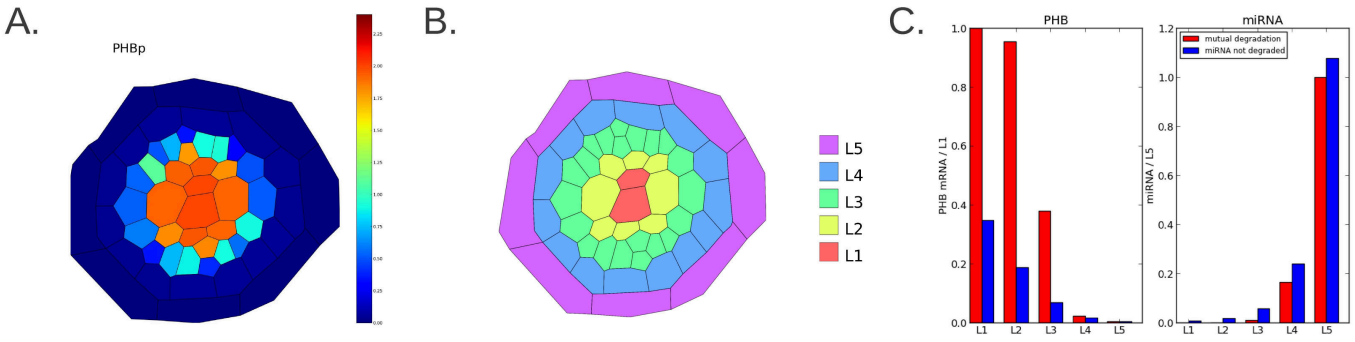

Figure 10: (A.) Steady state PHB protein in the wild type root cross section using the default parameter values in Table 3 with the original model (Equations (3) and (6)). (B.) Schematic root cross section showing cell layer groupings used to produce the mean value plots in C and in Figure 11. (C.) Mean *PHB* mRNA and miRNA in each of the cell layer groupings L1-L5 for both the original model (red), and the model given by Equations (7a) and (7b) in which miRNA is not degraded by the interaction with *PHB* mRNA (blue). For *PHB* mRNA each bar is plotted relative to the value in L1 using the original model, while for miRNA each bar is plotted relative to the value in L5 with the original model.

To demonstrate the importance of the mutual degradation of both the miRNA and *PHB* mRNA in establishing a sharp boundary to the domain of *PHB* expression an alternative model was considered in which while the miRNA still accelerates the degradation of *PHB* mRNA, it is itself no longer consumed in this reaction, as follows:

$$\begin{aligned}\frac{d[miRNA]_i}{dt} &= p_{miRNA} - d_{miRNA}[miRNA]_i \\ &\quad -\frac{1}{V_i}\sum_{n\in N_i} S_{i,n}P_{miRNA}\left([miRNA]_i - [miRNA]_n\right), \qquad (7a)\\ \frac{d[PHB_m]_i}{dt} &= p_{PHB_m} - d_{PHB_m}[PHB_m]_i \\ &\quad -d_{miRNA/mRNA}[PHB_m]_i[miRNA]_i, \qquad (7b)\end{aligned}$$

where the model variables and parameter values are as previously defined. For this alternative model the mean *PHB* mRNA in each cell layer L1-L5 is plotted, relative to the L1 value using the full model, for each of the parameter sets as shown in Figures 10(c) and 11. In each case, removing the mutual degradation of miRNA and *PHB* mRNA and replacing with just the miRNA promoted degradation of *PHB* mRNA removes the sharp boundary between strong and weak *PHB* expression in adjacent cell layers.

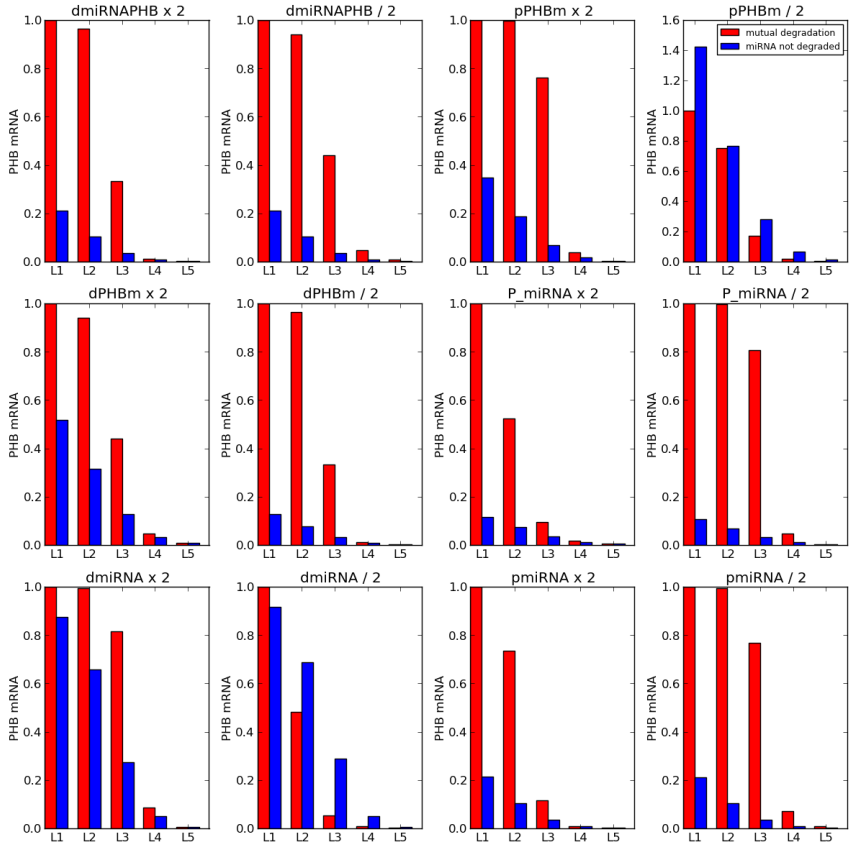

Figure 11: Alterations in parameter space in the *PHB* mRNA/miRNA submodel. Red bars: Mean steady state *PHB* mRNA using the original model (Equations (3) and (6)) in each of the cell layers L1-L5 (defined in Figure 10(b)), relative to the value in L1, for half and double each of the default parameter values for $d_{miRNA/mRNA}$, p_{PHB_m}, d_{PHB_m}, P_{miRNA}, d_{miRNA} and p_{miRNA} given in Table 3. In each case the remaining parameter values are kept to the default values. Blue bars: As for plot shown with red bars but using the model in which miRNA is not degraded by the interaction with *PHB* mRNA (Equations (7a) and (7b)). The bars are normalised to the value in L1 found using the original model.

2.1 Continuous approximation of the *PHB* - miRNA165/6 sub model

2.2 Model derivation

To examine further the relevance of mutual degradation in creating a sharp boundary of *PHB* mRNA we assumed that the root cross section has approximately radial symmetry with respect to geometry, production and degradation of *PHB* and miRNA and analyzed the evolution of $[\text{miRNA}](r,\theta,t)$ and $[\text{PHB}_m](r,\theta,t)$ on a circle of radius $\bar{R}$ with $r \in [0,\bar{R}]$, $\theta \in [0,2\pi]$ and $t \in \mathbb{R}^+$. We considered a two-dimensional discrete model comprising the interaction between miRNA and *PHB* mRNA and neglecting the other molecular interactions. The model assumes N_r cells along any radius for a fixed angle, N_θ cells along any circumference for a fixed radius and is given by the equations

$$\begin{aligned}\frac{\partial[miRNA](r,\theta,t)}{\partial t} &= p_{miRNA}(r) - d_{miRNA}[miRNA](r,\theta,t) - d_{miRNA/mRNA}[miRNA](r,\theta,t)[PHB_m](r,\theta,t) \\ &\quad + D\Delta_d[miRNA](r,\theta,t), \qquad (8a)\\ \frac{\partial[PHB_m](r,\theta,t)}{\partial t} &= p_{PHB_m} - d_{PHB_m}[PHB_m](r,\theta,t) - d_{miRNA/mRNA}[miRNA](r,\theta,t)[PHB_m](r,\theta,t), \qquad (8b)\end{aligned}$$

where Δ_d is a discrete Laplacian operator accounting for the circular geometry,

$$\begin{aligned}\Delta_d[miRNA](r,\theta,t) &:= \frac{[miRNA](r-\delta_r,\theta,t) - 2[miRNA](r,\theta,t) + [miRNA](r+\delta_r,\theta,t)}{\delta_r^2} \\ &\quad + \frac{1}{r}\frac{[miRNA](r+\delta_r,\theta,t) - [miRNA](r-\delta_r,\theta,t)}{2\delta_r} \\ &\quad + \frac{1}{r^2}\frac{[miRNA](r,\theta-\delta_\theta,t) - 2[miRNA](r,\theta,t) + [miRNA](r,\theta+\delta_\theta,t)}{\delta_\theta^2}, \qquad (9)\end{aligned}$$

D is the diffusion coefficient of $[miRNA]$, $r = i \cdot \delta_r = i \cdot \frac{\bar{R}}{N_r}$ and $\theta = j \cdot \delta_\theta = j \cdot \frac{2\pi}{N_\theta}$, where $i = 1, \ldots, N_r$ and $j = 1, \ldots, N_\theta$ are the cell indexes, δ_r, δ_θ are the radial and angular spacings, and where reactions and parameters are defined as in Section 1. Approximate estimates measured from cross sections in root regions similar to the one represented in Supplementary Figure 1 suggest that on average $\bar{R} = 45\ \mu m$. We assume that miRNA is transcribed in a region close to the boundaries, representing the endodermis, at rate:

$$p_{miRNA}(r) := \begin{cases} 32.5\ \mu M \cdot s^{-1} & \text{if } 0\ \mu m \leq r \leq 5\ \mu m \text{ or } 40\ \mu m \leq r \leq 45\ \mu m, \\ 0\ \mu M \cdot s^{-1} & \text{if } 5\ \mu m \leq r \leq 40\ \mu m. \end{cases}$$

Accounting for radial symmetry and assuming that $\delta_r, \delta_\theta \ll 1$, we then derive a continuum limit and analyze how the steepness of $[PHB_m]$ profile varies when we vary the degradation rate $d_{miRNA/mRNA}$ in two model variants. In the first variant, we assume that miRNA and *PHB* mRNA mutually degrade one another following the equations:

$$\begin{aligned} \frac{\partial [miRNA](r,t)}{\partial t} &= p_{miRNA}(r) - d_{miRNA}[miRNA](r,t) \\ &\quad -d_{miRNA/mRNA}[miRNA](r,t)[PHB_m](x,t) + D\Delta[miRNA](r,t), \qquad (10a) \\ \frac{\partial [PHB_m](r,t)}{\partial t} &= p_{PHB_m} - d_{PHB_m}[PHB_m](r,t) - d_{miRNA/mRNA}[miRNA](r,t)[PHB_m](r,t), \qquad (10b) \end{aligned}$$

where Δ is the usual Laplacian operator, namely in the radially symmetric case

$$\Delta[miRNA](r,t) = \frac{\partial^2 [miRNA]}{\partial r^2} + \frac{1}{r}\frac{\partial [miRNA]}{\partial r}, \qquad (11)$$

with $0 < r < \bar{R}$, with the following conditions at $r = 0, \bar{R}$

$$\begin{aligned} \frac{\partial [miRNA](\bar{R},t)}{\partial r} &= 0, \qquad (12a) \\ |[miRNA](0,t)| &< \infty, \qquad (12b) \end{aligned}$$

and with initial conditions given by

$$[miRNA](r,0) = 0, \qquad [PHB_m](r,0) = 0. \qquad (13)$$

In the second variant we assume that only *PHB* mRNA is degraded by miRNA as follows:

$$\begin{aligned} \frac{\partial [miRNA](r,t)}{\partial t} &= p_{miRNA}(r) - d_{miRNA}[miRNA](r,t) + D\Delta[miRNA](r,t), \qquad (14a) \\ \frac{\partial [PHB_m](r,t)}{\partial t} &= p_{PHB_m} - d_{PHB_m}[PHB_m](r,t) - d_{miRNA/mRNA}[miRNA](r,t)[PHB_m](r,t), \qquad (14b) \end{aligned}$$

with the boundary and initial conditions given by Eqs. (12), (13).

2.3 Analytical solutions

The time dependent solution of equation (14a) and the steady states of equations (14) can be derived analytically. The steady state of equation (14a) follows by substituting into the equation

$$0 = p_{miRNA}(r) - d_{miRNA}[miRNA](r) + D\Delta[miRNA](r) \qquad (15)$$

the Fourier-Bessel series expansions

$$p_{miRNA}(r) := \sum_{n=0}^{\infty} p_n J_0(\lambda_n r), \qquad [miRNA](r) := \sum_{n=0}^{\infty} m_n J_0(\lambda_n r), \qquad (16)$$

where $J_0(\lambda_n r)$ is the zero-th Bessel function of the first kind, $0 < \lambda_0 < \ldots < \lambda_n < \ldots$ are the infinite solutions of the equation $J_0'(\lambda_n \bar{R}) = 0$ and

$$p_n := \frac{\langle p_{miRNA}(r), J_0(\lambda_n r)\rangle}{\|J_0(\lambda_n r)\|^2}, \qquad m_n := \frac{\langle [miRNA](r), J_0(\lambda_n r)\rangle}{\|J_0(\lambda_n r)\|^2}$$

are the coefficients of the Fourier-Bessel series with

$$\langle f(r), g(r)\rangle := \int_0^{\bar{R}} f(r)g(r)rdr, \qquad \|f\|^2 := \langle f, f\rangle, \qquad f, g : (0, \bar{R}] \to \mathbb{R}.$$

From the identity $\Delta J_0(\lambda_n r) = -\lambda_n^2 J_0(\lambda_n r)$ it follows that $m_n = \frac{p_n}{D\lambda_n^2 + d_{miRNA}}$ and, from the latter, we deduce that the steady state solution is given by

$$[miRNA](r) = \sum_{n=0}^{\infty} \frac{p_n}{D\lambda_n^2 + d_{miRNA}} J_0(\lambda_n r). \tag{17}$$

The corresponding time dependent solution is

$$[miRNA](r) = \sum_{n=0}^{\infty} p_n \frac{1 - e^{-(D\lambda_n^2 + d_{miRNA})t}}{D\lambda_n^2 + d_{miRNA}} J_0(\lambda_n r). \tag{18}$$

At steady state, equation (14b) supplies an algebraic equation for $[PHB_m]$ in terms of $[miRNA]$ which can be written as

$$[PHB_m](r) = \frac{p_{PHB_m}}{d_{PHB_m} + d_{miRNA/mRNA}[miRNA](r)}.$$

The case with mutual degradation of *PHB* mRNA and miRNA given by equations (10) cannot be solved analytically (cf. Levine et al. [6]) but it can be clarified further by an asymptotic analysis of the limit in which $d_{miRNA/mRNA}$ becomes large, so that miRNA and *PHB* mRNA cannot coexist at significant levels at the same location. In this case, a sharp-interface problem then results in the limit, with sharp drops off in miRNA and *PHB* mRNA levels either side of the interface. In particular, if

$$d_{miRNA/mRNA}[miRNA] \gg d_{PHB_m}, \tag{19}$$

then in the miRNA rich region and at steady state, on neglecting the independent degradation term in Eq. (10b) one has

$$p_{miRNA}(r) - p_{PHB_m} - d_{miRNA}[miRNA](r) + D\Delta[miRNA](r) = 0. \tag{20}$$

Although formally the solution of Eq. (20) on the full domain reduces to Eq. (17) with

$$p_n = \frac{\langle p_{miRNA}(r) - p_{PHB_m}, J_0(\lambda_n r)\rangle}{\|J_0(\lambda_n r)\|^2} \tag{21}$$

this solution approximates the steady state solution of Eq. (10a) only in the region satisfying the condition (19). Conversely, assuming that in the *PHB* mRNA rich region the effect of miRNA diffusion is negligible and that at any cellular position the decay of miRNA and *PHB* mRNA is dominated by coupled degradation within a 'strong interaction limit' defined by the inequality

$$\max\left\{\frac{d_{miRNA/mRNA} \cdot p_{miRNA}(r)/d_{miRNA}}{d_{PHB_m}}, \frac{d_{miRNA/mRNA} \cdot p_{PHB_m}/d_{PHB_m}}{d_{miRNA}}\right\} \gg 1, \qquad \forall r \tag{22}$$

the estimate of PHB mRNA concentration at steady state derived in one dimension (cf. Levine et al. [6]) for an mRNA concentration of an unspecified gene under these conditions still holds in two dimensions:

$$[PHB_m](r) \approx \frac{[p_{PHB_m} - p_{miRNA}(r)]_+}{d_{PHB_m}}, \tag{23}$$

with $[x]_+ = \max\{0, x\}$.

2.4 Numerical solutions

In order to express the steepness of $[PHB_m]$ quantitatively we calculated numerically its spatial derivative $\frac{\partial[PHB_m]}{\partial x}$ on a diameter $D = [-\bar{R}, \bar{R}]$ at a point $\bar{x} \in I = [-\bar{R}, 0]$ such that

$$[PHB_m](\bar{x}) = \frac{\max_{x\in I}([PHB_m]) + \min_{x\in I}([PHB_m])}{2}$$

and we considered its absolute value $\left|\frac{\partial[PHB_m]}{\partial x}(\bar{x})\right|$ as an estimate of $[PHB_m]$ sharpness. In both variants we maintained transcription and degradation rates as defined in Supplementary Tables 2, 3 and we fixed $D = 1.5\ \mu m^2 \cdot s^{-1}$. In Figure 12a we show the steady state solutions of equations (10) and (14) together with a segment which is tangent to $[PHB_m]$ at $\bar{x}$. The slope of this segment is clearly higher when mutual degradation occurs. The importance of mutual degradation in generating a steep gradient of $[PHB_m]$ is further highlighted in Figure 12b which shows how PHB sharpness ($\left|\frac{\partial[PHB_m]}{\partial x}(\bar{x})\right|$) varies in the steady state solutions of equations (10) and (14) when changing $d_{miRNA/mRNA}$. Whereas PHB sharpness reaches a plateau at higher values of $d_{miRNA/mRNA}$ when miRNA is not degraded by *PHB* mRNA, mutual degradation causes a pronounced increase in $\left|\frac{\partial[PHB_m]}{\partial x}(\bar{x})\right|$ when increasing $d_{miRNA/mRNA}$.

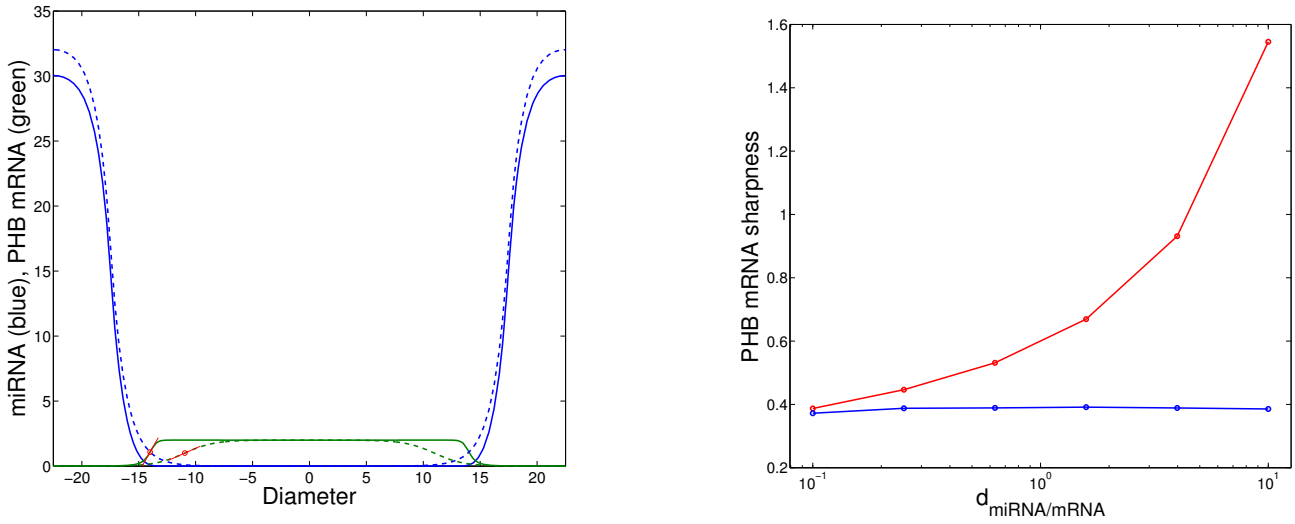

(a) (b)

Figure 12: Continuous approximation of the PHB - miRNA165/6 sub model. (a) Steady state solutions of Eqs. (10) (solid lines) and (14) (dashed lines) along a diameter. Steady state solutions of miRNA are presented in blue, whereas steady state solutions of *PHB* mRNA are shown in green. The red segments are tangent to $[PHB_m]$ at $\bar{x}$ and their slope highlights that when mutual degradation is present the profile of *PHB* mRNA is steeper. (b) *PHB* mRNA sharpness ($\left|\frac{\partial[PHB_m]}{\partial x}(\bar{x})\right|$) of the steady state solutions of Eqs. (10) (red line) and (14) (blue line) at increasing values of $d_{miRNA/mRNA}$. Mutual degradation causes *PHB* mRNA sharpness to increase more dramatically than when miRNA is not degraded by *PHB* mRNA.

3 Sensitivity analysis

Mathematical models of signaling networks often comprise of a large number of nonlinear differential equations describing the interaction network which, in turn, rely upon a large number of parameters associated with the reaction rates. Since the input/output relationships in such models may be not intuitive, sensitivity analysis algorithms may help identifying which parameters play a key role by ordering the relevance of parameter variations (input) in modifying the variation in the model variables (output). In order to investigate how the variables of the mathematical model defined by Eqs. (1)-(6) vary when choosing parameter values that differ from the default value reported in Supplementary Tables 2 and 3 we apply three types of sensitivity analysis.

Firstly, using a local sensitivity analysis, we analyze in one-dimension how each individual component of the sub-cellular interaction network is affected by variation of each parameter from its default value, in two representative tissue types (inside and outside the metaxylem), allowing us to identify which variables are most affected by parameter perturbations. The parameters are then ranked by the average sensitivity of the model variables to parameter perturbations allowing us to identify which parameters have the strongest influence on the components of the interaction network.

We then apply a global sensitivity analysis, which ranks the sensitivity of parameters over a much wider region of the parameter space. This finds that, in general, the parameters whose rankings in the global analysis differ most from those computed by the local analysis are ranked lower by the local sensitivity algorithm than the global sensitivity algorithm. This suggests that their optimised values do not reside within a sensitive region of the

parameter space and that the signalling pathway is relatively robust to parameter variation [14].

We finally select the parameters that affect the variables of the sub-cellular network most strongly, and analyze the sensitivity of the model variables in every tissue within the full multicellular model to variation in these parameters.

3.1 Sub-cellular network (local sensitivity analysis).

Following the approach proposed in [15], [16], we analyse the steady state sensitivity of the sub-cellular interactions defined by Eqs. (1)-(6) to perturbations from the default set reported in Supplementary Tables 2 and 3, with the exception of parameters associated with transport and permeability ($T_{Aux}, P_{Aux}, P_{Ck}, P_{miRNA}$) and parameters associated with PIN7 concentration (p_{PIN7_p}, d_{PIN7_p}). We have not included the endodermis in this analysis because it does not contain PIN7 and there is no significant variation in the expression of network components within this tissue.

Under these conditions, we can investigate two possibilities; namely, when a cell is located in the metaxylem (where CKIN is expressed) and when it is located outside this tissue (where CKIN is not expressed). The steady-state sensitivity for the k-th element (state or reaction rate) X_k with respect to the parameter p_j is defined by:

$$S_{k,j} := \frac{X_k^{(ss)}(p_j + \delta_{p_j}) - X_k^{(ss)}(p_j)}{\delta_{p_j}},$$

where $X_k^{(ss)}$ is the function returning the steady-state for this element (state or reaction rate) for the given parameter p_j and δ_{p_j} is a perturbation of this parameter [16]. The normalised sensitivity index, defined by:

$$S_{k,j}^{(n)} := \frac{p_j}{X_k^{ss}(p_j)} |S_{k,j}|, \tag{24}$$

estimates the sensitivity of the steady-state value $X_k^{(ss)}(p_j)$ to perturbation of the parameter p_j, relative to the absolute values of both the steady-state and the parameter under evaluation. This index is calculated for all the model species and parameters under a relative parameter perturbation of 1% as defined by default in the Systems Biology Toolbox for Matlab, SBToolbox [15]. Since nominal parameter values of zero lead to normalized sensitivities of zero for these parameters, and nominal steady-state values of zero lead to infinite normalised sensitivities, in these cases the normalized sensitivities for these parameters and states are not determined.

All parameters associated with cell geometry are set to zero, these being the transport and permeability parameters (T_{Aux}, P_{Aux}, P_{Ck}, P_{miRNA}) and parameters associated with PIN7 concentration (p_{PIN7_p}, d_{PIN7_p}). In addition, when considering a cell outside the metaxylem, parameters associated with CKIN (p_{CKIN_m}, p_{CKIN_p}, d_{CKIN_m}, d_{CKIN_p}, θ_{CKIN}, m_{CKIN}) are removed as this component is not present outside this tissue. The other parameter values are as reported in Supplementary Tables 2 and 3. The steady states represent changes in protein and mRNA levels when parameters are perturbed. The SBToolbox default relative parameter perturbation has been applied, this being set to be 1% of the parameter default value, [15]. The results of this evaluation for each parameter and model species, in typical cells outside and within the metaxylem, are given at http://www.cpib.ac.uk/vascularmodel, Figures 1-4.

In Supplementary Figure 13 we show a MinMax view of the magnitude of normalised steady-state sensitivities in a typical cell external to the metaxylem (Supplementary Figure 13a) and within the metaxylem (Supplementary Figure 13b). Bars extend from the minimal to the maximal values of all the sensitivities of the variables (species) of the model given by Eqs. (1)-(6) and reported in Supplementary Table 1. The names associated with the parameter ranks are reported in Supplementary Tables 4, 5. Blue lines show the mean value of the sensitivities of the model variables, whereas red lines their median value. Parameters are ranked by the mean values of the variable sensitivities in decreasing order.

The parameters that affect the average variable sensitivity the most outside the metaxylem are those associated with auxin expression and binding (see Supplementary Figure 13a and Supplementary Table 4). Within the metaxylem however, parameters associated with CKIN, auxin and cytokinin expression and binding have a stronger influence on the model output.

In Supplementary Table 6 we present the parameters that affect the average variable sensitivity the most in both cell types (inside and outside the metaxylem) by evaluating the sum of their ranks in the two cell types. We identify m_{Aux}, d_{Aux}, p_{Aux}, θ_{Aux}, p_{Ck}, d_{Ck}, θ_{Ck}, m_{Ck} as such parameters. Perturbation of these parameters will be analyzed include this parameter in the comparison among different tissues reported in Supplementary Table

Parameter rank	Parameter name	Parameter rank	Parameter name
1	m_{Aux}	19	d_{ARR5_p}
2	d_{Aux}	20	p_{miRNA}
3	θ_{Aux}	21	d_{miRNA}
4	p_{Aux}	22	θ_{ARR5}
5	d_{AHP6_m}	23	p_{PHB_m}
6	p_{AHP6_m}	24	p_{IAA2_m}
7	d_{AHP6_p}	25	d_{IAA2_m}
8	p_{AHP6_p}	26	$d_{miRNA/mRNA}$
9	θ_{AHP6}	27	p_{PHB_p}
10	m_{AHP6}	28	p_{PIN7_m}
11	p_{Ck}	29	p_{IAA2_p}
12	d_{Ck}	30	d_{PHB_p}
13	θ_{Ck}	31	d_{IAA2_p}
14	m_{Ck}	32	d_{PIN7_m}
15	m_{ARR5}	33	d_{PHB_m}
16	p_{ARR5_m}	34	m_{PHB}
17	d_{ARR5_m}	35	θ_{PHB}
18	p_{ARR5_p}		

Table 4: *Table summarising the parameter names associated to the parameter ranks reported in Supplementary Figure 13a.*

6; nevertheless, because of its high rank in the metaxylem we will also investigate the effect of its perturbation in two dimensions in section 3.3.

3.2 Sub-cellular network (global sensitivity analysis).

A local sensitivity analysis can provide information about the influence of varying parameters on the model output in a small range around chosen default parameters. In order to explore a much wider range of parameter choices, we now analyze the sensitivity of the same model used in the previous section by applying a variance-based global sensitivity algorithm.

In contrast to regression-based methods, variance-based methods do not assume linearity or monotonicity in the input-output relationships and are well suited to analyze models of non-linear differential equations [14]. Among these methods a well established algorithm is the eFAST algorithm [15], [14], [17], [18], [19].

The eFAST method is a variance decomposition method which partitions the variance of the model output, determining what fraction of the variance can be explained by variation in each input parameter [19]. The parameter space is sampled along curves defined by the transformation function:

$$\hat{x}_i = \frac{1}{2} + \frac{1}{\pi} \arcsin\left(\sin\left(\omega_i y + \phi_i\right)\right),$$

where each parameter varies at frequency ω_i and random phase shift ϕ_i with a scalar variable $y \in (-\pi, \pi)$. With this transformation the model output function can be expressed as a Fourier series with respect to y [14].

The overall variance of the output function is decomposed into summands of the square of Fourier series coefficients which are calculated by Monte Carlo integrations on the sampled parameter space. As a result of this decomposition, two sensitivity indexes are then defined for each parameter: a first-order sensitivity index and a total effect sensitivity index. The first-order sensitivity index S_i of a parameter i is calculated as the variance at the frequency uniquely associated with a parameter divided by the total variance. More precisely, the variance s_i^2 is firstly calculated from the Fourier coefficients at the frequency of interest, the first-order sensitivity index S_i is then defined as

$$S_i = \frac{s_i^2}{s_{total}^2}$$

The first-order sensitivity index represents the fraction of the model output variance which is explained by the input variation of a given parameter. The total effect sensitivity index S_{T_i} is then estimated as follows. eFAST first computes the summed sensitivity index of the entire complementary set of parameters, namely the set of all

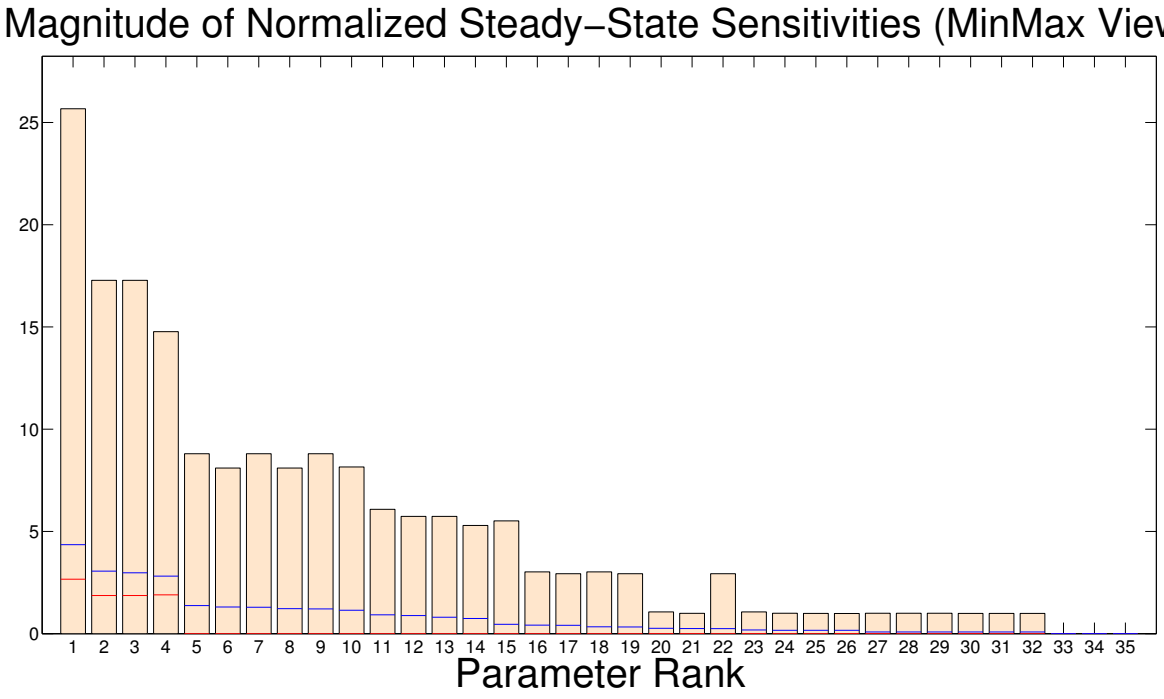

(a)

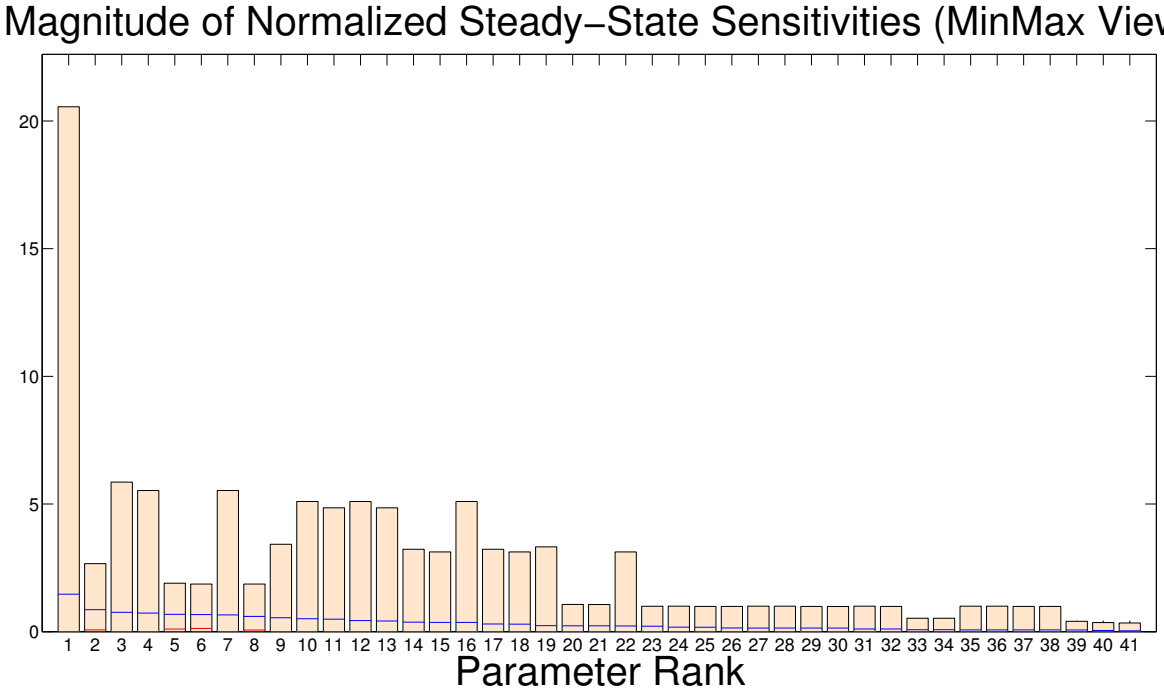

(b)

Figure 13: MinMax view of the magnitude of normalized steady-state sensitivities in a typical cell external to the metaxylem (a) and within the metaxylem (b). Bars extend from the minimal to the maximal values of all the sensitivities of the variables (species) of the model given by Eqs. (1)-(6) and reported in Supplementary Table 1. The names associated with the parameter ranks are reported in Supplementary Tables 4, 5. Blue lines show the mean value of the model variables, whereas red lines their median value.

Parameter rank	Parameter name	Parameter rank	Parameter name
1	m_{CKIN}	22	θ_{ARR5}
2	m_{Aux}	23	d_{miRNA}
3	p_{Ck}	24	p_{AHP6_m}
4	d_{Ck}	25	d_{AHP6_m}
5	p_{Aux}	26	d_{PHB_p}
6	d_{Aux}	27	p_{PHB_p}
7	θ_{Ck}	28	p_{IAA2_m}
8	θ_{Aux}	29	d_{IAA2_m}
9	m_{Ck}	30	$d_{miRNA/mRNA}$
10	d_{CKIN_m}	31	p_{AHP6_p}
11	p_{CKIN_m}	32	d_{AHP6_p}
12	d_{CKIN_p}	33	d_{PHB_m}
13	p_{CKIN_p}	34	θ_{PHB}
14	p_{ARR5_m}	35	p_{PIN7_m}
15	d_{ARR5_m}	36	p_{IAA2_p}
16	θ_{CKIN}	37	d_{PIN7_m}
17	p_{ARR5_p}	38	d_{IAA2_p}
18	d_{ARR5_p}	39	m_{AHP6}
19	m_{ARR5}	40	m_{PHB}
20	p_{PHB_m}	41	θ_{AHP6}
21	p_{miRNA}		

Table 5: *Table summarising the parameter names associated to the parameter ranks reported in Supplementary Figure 13b.*

Parameter name	Parameter rank not in metaxylem	Parameter rank in metaxylem	Sum of ranks (< 30)
m_{Aux}	1	2	3
d_{Aux}	2	6	8
p_{Aux}	4	5	9
θ_{Aux}	3	8	11
p_{Ck}	11	3	14
d_{Ck}	12	4	16
θ_{Ck}	13	7	20
m_{Ck}	14	9	23

Table 6: *Table summarising the most sensitive parameters in a cell within and outside the metaxylem as evaluated by the sum of the parameter ranks in both tissues. Parameters whose sum of ranks is minor than the arbitrary threshold of* 30 *are reported, these being associated with auxin and cytokinin expression and binding.*

parameters except for parameter i. S_{T_i} is then calculated as the remaining variance after the contribution of the complementary set S_{ci} is removed:

$$S_{T_i} = 1 - S_{ci}$$

In such a way, S_{T_i} evaluates also higher-order, nonlinear interactions between the parameter of interest and the complementary set of parameters.

In what follows we evaluate the total effect sensitivity indexes of the model variables considering the two subcellular cases and nominal parameter values that we analyzed in the previous section. More precisely, we applied the eFAST algorithm as encoded in the Systems Biology Toolbox for Matlab, SBToolbox [15] by maintaining the default algorithm parameter values (1000 Monte Carlo simulations, one order of magnitude of parameters range from the nominal parameter value).

Since data showing a high degree of cooperativity have Hill coefficients of up to 10 [20], [21] and a perturbation of one order of magnitude would lead to Hill coefficients up to 50, we do not include in the global sensitivity analysis these parameters. Perturbations of the Hill coefficients from their nominal values were however investigated locally in the previous section.

As with the local sensitivity analysis, in Supplementary Figure 14 we show a MinMax view of the magnitude of the total effect sensitivities in a typical cell external to the metaxylem (Supplementary Figure 14a) and within the metaxylem (Supplementary Figure 14b). Bars extend from the minimal to the maximal values of all the sensitivities of the variables (species) of the model given by Eqs. (1)-(6) and reported in Supplementary Table 1. The names associated with the parameter ranks are reported in Supplementary Tables 7 and 8. Blue lines show the mean value of the model variables, whereas red lines their median value.

Because of the variation in the search space between the local and global sensitivity analyses, the relative influence of parameter perturbations on the model variables, which we evaluate as parameter ranks, may differ between the two. Supplementary Table 9 lists the parameters outside the metaxylem with the greatest difference in rank between the two analyses (> 10 ranks), and Supplementary Table 10 lists those parameters that differ most in rank within the metaxylem. Comparing the ranking of the parameter sensitivities of the local analysis with the global analysis in this way, we found that in general, the parameters whose rankings differ most between the two analyses are ranked lower by the local sensitivity algorithm than the global sensitivity algorithm.

The result of this comparitive analysis means that the parameters whose associated sensitivity is most influenced by increasing the search space of their perturbed values are relatively less sensitive to local perturbations around their default value than to global perturbations comprising a wider parameter range, suggesting that their default values do not reside within a sensitive region of the parameter space. Consequently, the signalling pathway appears to be operating in a region of parameter space more robust to stochastic variation in gene regulation affecting these parameters [14] than if their default values were chosen in other regions of the search space.

In cases where the difference in ranked influence between the global and local sensitivity is small, this suggests that the parameters sampled in the smaller search space in the local analysis do not have a greater relative influence on the model output than when parameters are sampled in the wider search space using the global sensitivity algorithm. In other words, in relative terms, the choice of the default parameter values is not greatly affecting the sensitivity of the model to small perturbations in these parameters.

3.3 2D model of vascular patterning.

Using the results of the sensitivity analysis of the one-dimensional model developed in sections 3.1, 3.2, we now evaluate in our multicellular model given by Eqs. (1)-(6), and the tissue representation reported in Supplementary Figures 1 and 2, the sensitivities of the parameters that most effect the model variables in one dimension, both in the metaxylem and outside the metaxylem. The selected parameters are p_{Aux}, p_{Ck}, d_{Aux}, d_{Ck}, θ_{Aux}, θ_{Ck}, m_{Aux}, m_{Ck} and m_{CKIN}, the latter of which is most important in the metaxylem. We also analyze perturbations in transport, permeability, PIN7 protein production and protein degradation rates, as these were not included in the 1D sensitivity analysis, and the parameters affecting mutual degradation of *PHB* mRNA and miRNA165/6 as a further support of the analysis performed in Section 2. Parameters were perturbed 10% above their default values reported in Supplementary Tables 2 and 3.

In Supplementary Figures 16 - 18 we show the mean of the normalized sensitivity index given by Eq. (24) for all cells of each cell type, calculated for each model component, for each parameter listed above. As expected intuitively, p_{Aux} and d_{Aux} play the strongest role in the sensitivity of auxin and of the proteins associated with auxin response (IAA2, AHP6), and p_{CK} and d_{CK} influence mainly the sensitivity of cytokinin, ARR5 and PIN7. Parameters associated with protein-DNA binding and Hill coefficients present an analogous effect on the network

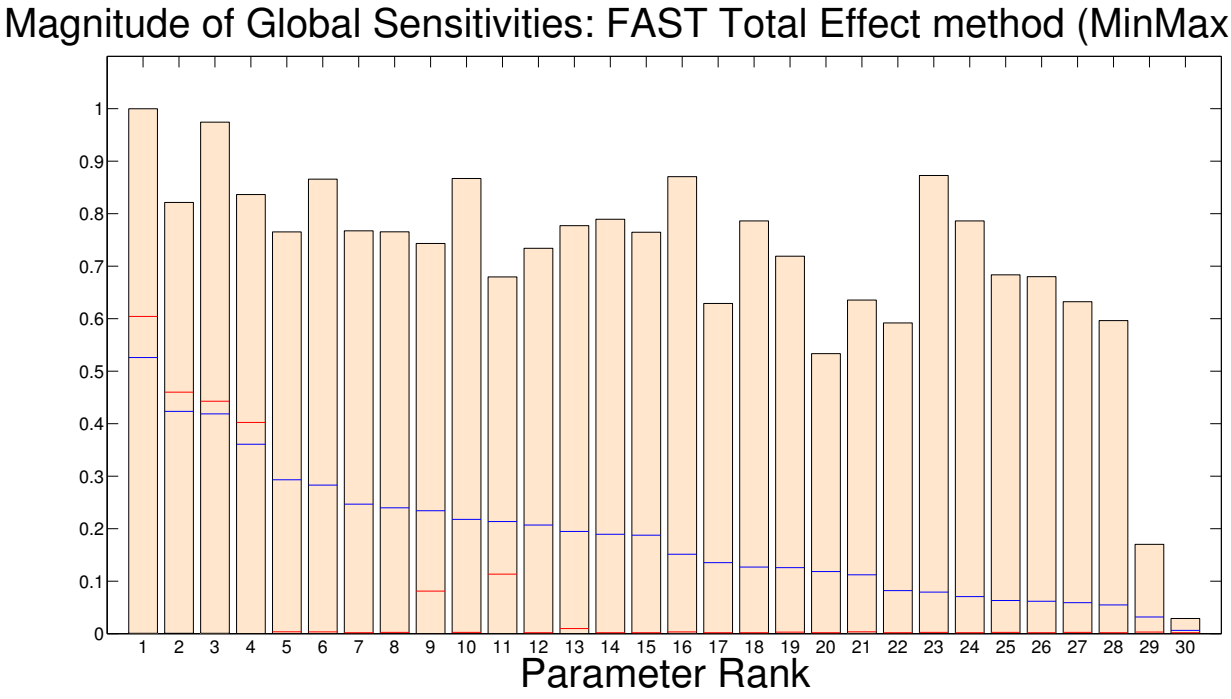

(a)

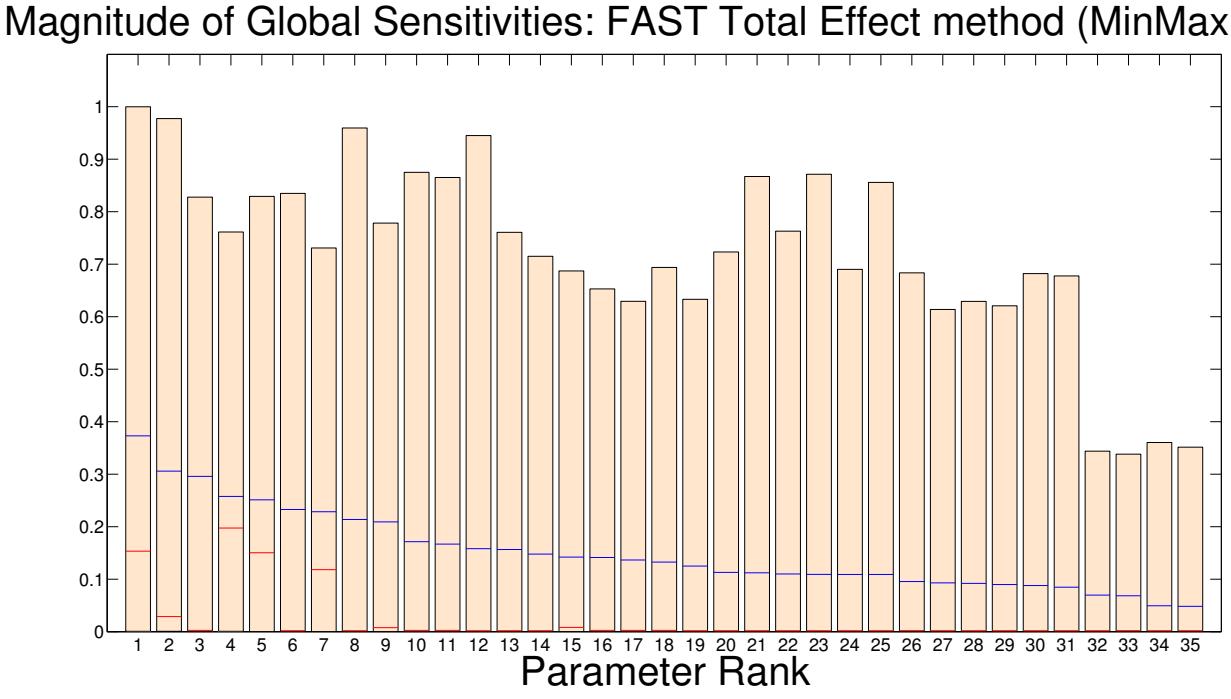

(b)

Figure 14: MinMax view of the magnitude of the total effect sensitivities in a typical cell outside the metaxylem (a) and within the metaxylem (b). Bars extend from the minimal to the maximal values of all the sensitivities of the variables (species) of the model given by Eqs. (1)-(6) and reported in Supplementary Table 1. The names associated with the parameter ranks are reported in Supplementary Tables 7, 8. Blue lines show the mean value of the model variables, whereas red lines their median value.

Parameter rank	Parameter name	Parameter rank	Parameter name
1	d_{Aux}	16	d_{IAA2_m}
2	p_{Aux}	17	p_{ARR5_m}
3	θ_{Aux}	18	$d_{miRNA/mRNA}$
4	p_{PHB_m}	19	d_{ARR5_p}
5	p_{AHP6_m}	20	θ_{AHP6}
6	d_{AHP6_m}	21	p_{IAA2_m}
7	d_{Ck}	22	p_{ARR5_p}
8	p_{AHP6_p}	23	d_{IAA2_p}
9	d_{miRNA}	24	d_{PIN7_m}
10	d_{AHP6_p}	25	d_{PHB_p}
11	p_{PHB_p}	26	θ_{ARR5}
12	p_{Ck}	27	p_{IAA2_p}
13	p_{miRNA}	28	p_{PIN7_m}
14	d_{ARR5_m}	29	d_{PHB_m}
15	θ_{Ck}	30	θ_{PHB}

Table 7: *Table summarising the parameter names associated to the parameter ranks reported in Supplementary Figure 14a.*

Parameter rank	Parameter name	Parameter rank	Parameter name
1	d_{Aux}	19	θ_{CKIN}
2	θ_{Aux}	20	p_{ARR5_m}
3	p_{CKIN_m}	21	d_{ARR5_p}
4	p_{Aux}	22	d_{IAA2_p}
5	p_{PHB_m}	23	d_{PIN7_m}
6	p_{CKIN_p}	24	p_{AHP6_p}
7	d_{miRNA}	25	d_{AHP6_p}
8	p_{miRNA}	26	d_{CKIN_p}
9	d_{Ck}	27	d_{PHB_p}
10	d_{IAA2_m}	28	p_{IAA2_p}
11	d_{AHP6_m}	29	p_{PIN7_m}
12	d_{ARR5_m}	30	p_{ARR5_p}
13	$d_{miRNA/mRNA}$	31	p_{Ck}
14	θ_{Ck}	32	θ_{ARR5}
15	p_{PHB_p}	33	d_{PHB_m}
16	p_{IAA2_m}	34	θ_{AHP6}
17	d_{CKIN_m}	35	θ_{PHB}
18	p_{AHP6_m}		

Table 8: *Table summarising the parameter names associated to the parameter ranks reported in Supplementary Figure 14b.*

Parameter name	Parameter rank in local analysis	Parameter rank in global analysis	Distance by ranks (>10 ranks)
p_{PHB_m}	23	4	19
p_{PHB_p}	27	11	16
d_{miRNA}	21	9	12
θ_{AHP6}	9	20	11

Table 9: *Table summarising the parameters whose local sensitivity rankings differ most from the global rankings (>10 ranks) in decreasing order of difference in a cell outside the metaxylem.*

Parameter name	Parameter rank in local analysis	Parameter rank in global analysis	Distance by ranks (> 10 ranks)
p_{Ck}	3	31	28
d_{IAA2_m}	29	10	19
$d_{miRNA/mRNA}$	30	13	17
d_{miRNA}	23	7	16
d_{IAA2_p}	38	22	16
p_{PHB_m}	20	5	15
d_{AHP6_m}	25	11	14
d_{PIN7_m}	37	23	14
d_{CKIN_p}	12	26	14
p_{miRNA}	21	8	13
p_{ARR5_p}	17	30	13
p_{PHB_p}	27	15	12
p_{IAA2_m}	28	16	12

Table 10: *Table summarising the parameters whose local sensitivity rankings differ most from the global rankings (> 10 ranks) in decreasing order of difference in a cell within the metaxylem.*

components, with θ_{Aux} and m_{Aux} influencing mostly IAA2 and AHP6 sensitivity, and with θ_{CK} and m_{Ck} affecting mainly ARR5 and PIN7 (see Supplementary Figure 16).

In Supplementary Figure 15 we show the same chart when perturbing m_{CKIN}. As it can be observed by the magnitude of the mean normalized sensitivity (of the order of 10^{-8}), the sensitivity of the model variables across different tissues of the cross-section to m_{CKIN} in the two-dimensional model is not as noteworthy as in the one-dimensional model in a single cell within the metaxylem.

We then analyzed the sensitivity of the model variables to changes in parameters that are associated with the cellular geometry that could not be analyzed in the one-dimensional model. Supplementary Figure 17 shows the mean normalized sensitivities of the two-dimensional model when perturbing T_{Aux}, P_{Aux}, P_{Ck}, P_{miRNA}, p_{PIN7_p} and d_{PIN7_p}. Perturbations in T_{Aux}, P_{Aux} influence mainly the sensitivity of auxin, IAA2 and AHP6, with T_{Aux} playing a stronger role in phloem, procambial and xylem cells, while perturbations in P_{Ck} affects mainly cytokinin, ARR5 and PIN7, and perturbations in P_{miRNA} act mostly on miRNA, PHB and AHP6.

In Section 2 the robustness of a sub-model of *PHB* mRNA and miRNA165/6 mutual degradation was investigated by varying the parameter values associated and observing the spatial pattern generated. We extend this here by analysing the sensitivity of these parameters in the full model given by Eqs. (1)-(6). Supplementary Figure 18 shows the mean normalized sensitivities of the two-dimensional model when perturbing p_{miRNA}, p_{PHB_m}, d_{miRNA}, d_{PHB_m} and $d_{miRNA/mRNA}$. As expected intuitively, perturbations in these parameters affect mainly the network components that they regulate directly ($miRNA$, PHB_p) or indirectly ($AHP6_p$, $ARR5_p$), in the tissues in which these components are present.

The simulation results at $t = 15$ seconds of our multicellular model given by Eqs. (1)-(6), the tissue representation reported in Supplementary Figures 1 and 2 and the default parameter values reported in Supplementary Tables 2 and 3 show that vascular patterning is maintained under all the parameter perturbations discussed in this section. The model output under each of these perturbations is given at http://www.cpib.ac.uk/vascularmodel, Figures 5-24.

4 Steady state analysis

In order to establish and maintain a pattern of gene expression when PIN is free to be expressed throughout the root vasculature, with a homogeneous production rate of both auxin and cytokinin, it must be possible for adjacent cells of a similar size and shape to have significantly different steady state expression of key genes. This can be tested using the model by finding the possible steady states as key model parameters are varied. In particular, the existence of multiple possible steady states within a cell for given production rates of auxin and cytokinin would demonstrate the possibility that a pattern of gene expression within a field of cells could be produced.

It is not practical to compute steady states in the full model with all the spatial information, either analytically or numerically, so to investigate further a number of model simplifications are made. Firstly, rather than the full

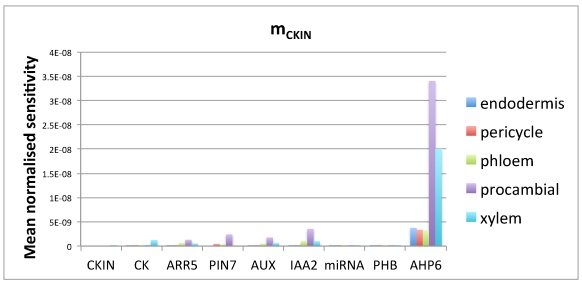

Figure 15: Plot representing the mean, calculated for all cells in a particular tissue and for all tissues, of the normalised sensitivity index given by Eq. (24) when perturbing m_{CKIN} 10% above its default value reported in Supplementary Table 3. The sensitivity of the model variables across different tissues to m_{CKIN} is not as noteworthy as in the one-dimensional model in a single cell within the metaxylem being of the order of magnitude of 10^{-8}.

spatial tissue structure, we consider just two cells of equal volume, with a single interface of unit area between the two. A value for the cell volume of $V = 6$ is used as an approximation of the mean wall surface area to volume ratio found in the full tissue structure. We also assume that the level of PIN at the cell membrane facing the shared interface of a cell i at any time is equal to the level of of PIN protein ($[PIN_p]_i$) present in cell i at that time.

While the spatial distributions of both cytokinin and PHB protein are governed by the full model, neither are regulated directly or indirectly in the model by auxin or the genes $AHP6$, $PIN7$ or $ARR5$. Because of this, to investigate model steady states both cytokinin (Ck) and PHB protein (PHB) are considered as parameter inputs to a simplified sub-model governing $AHP6$, $PIN7$ and $ARR5$. The initial values for Ck and PHB used are the approximate values seen in the xylem pole pericycle cells in the full spatial model, using the default parameter set ($Ck = 0.2$, $PHB = 0.5$). The affect of changing these parameters is investigated in the steady state analysis. Finally, it is not necessary to include $IAA2$ in the model when analyzing the steady states of genes regulating xylem pole specification because it doesn't regulate the output of any other components. If the cells in the simplified model are denoted by their subscript, we have the following model:

$$\begin{aligned}
\frac{d[Aux]_1}{dt} &= p_{Aux} - d_{Aux}[Aux]_1 - \frac{P_{Aux}}{V}\left([Aux]_1 - [Aux]_2\right) \\
&\quad - \frac{T_{Aux}}{V}\left([PIN7_p]_1[Aux]_1 - [PIN7_p]_2[Aux]_2\right), && \text{(25a)} \\
\frac{d[Aux]_2}{dt} &= p_{Aux} - d_{Aux}[Aux]_2 - \frac{P_{Aux}}{V}\left([Aux]_2 - [Aux]_1\right) \\
&\quad - \frac{T_{Aux}}{V}\left([PIN7_p]_2[Aux]_2 - [PIN7_p]_1[Aux]_1\right), && \text{(25b)} \\
\frac{d[AHP6_m]_i}{dt} &= p_{AHP6_m}F^{(i)}_{AHP6_m} - d_{AHP6_m}[AHP6_m]_i, && \text{(25c)} \\
\frac{d[ARR5_m]_i}{dt} &= p_{ARR5_m}F^{(i)}_{ARR5_m} - d_{ARR5_m}[ARR5_m]_i, && \text{(25d)} \\
\frac{d[PIN7_m]_i}{dt} &= p_{PIN7_m}F^{(i)}_{PIN7_m} - d_{PIN7_m}[PIN7_m]_i, && \text{(25e)} \\
\frac{d[AHP6_p]_i}{dt} &= p_{AHP6_p}[AHP6_m]_i - d_{AHP6_p}[AHP6_p]_i, && \text{(25f)} \\
\frac{d[ARR5_p]_i}{dt} &= p_{ARR5_p}[ARR5_m]_i - d_{ARR5_p}[ARR5_p]_i, && \text{(25g)} \\
\frac{d[PIN7_p]_i}{dt} &= p_{PIN7_p}[PIN7_m]_i - d_{PIN7_p}[PIN7_p]_i, && \text{(25h)}
\end{aligned}$$

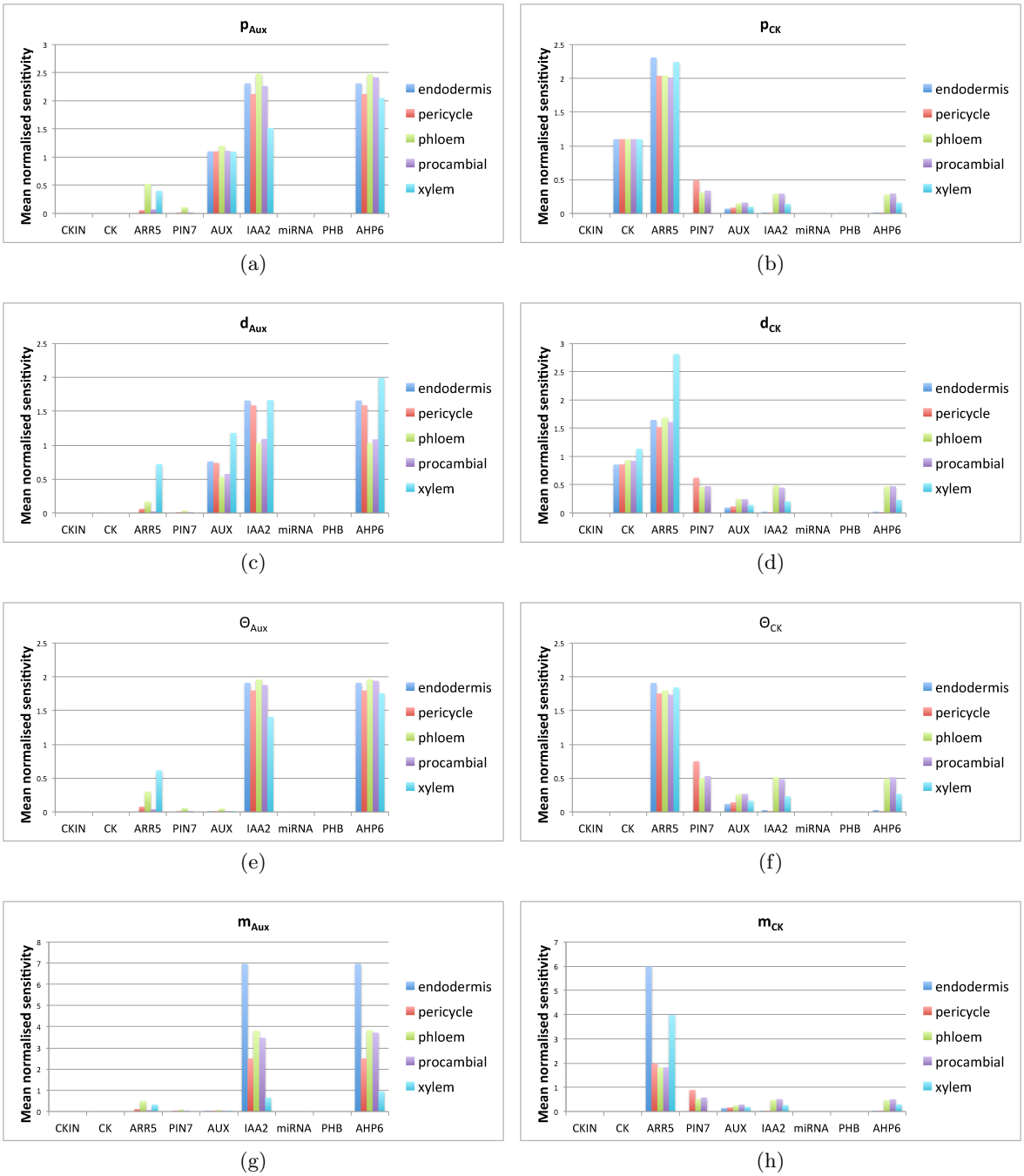

Figure 16: Series of plots representing the mean, calculated for all cells in a particular tissue and for all tissues, of the normalized sensitivity index given by Eq. (24). Parameters associated with auxin and cytokinin expression and binding (p_{Aux}, p_{CK}, d_{Aux}, d_{CK}, θ_{Aux}, θCK, m_{Aux}, m_{CK}) are perturbed 10% above their default value reported in Supplementary Tables 2 and 3. As expected intuitively perturbations in these parameters affect mainly the network components that they regulate directly or indirectly (auxin, IAA2, AHP6 for parameters associated with auxin; cytokinin, ARR5, PIN7 for parameters associated with cytokinin) in the tissues in which these components are present.

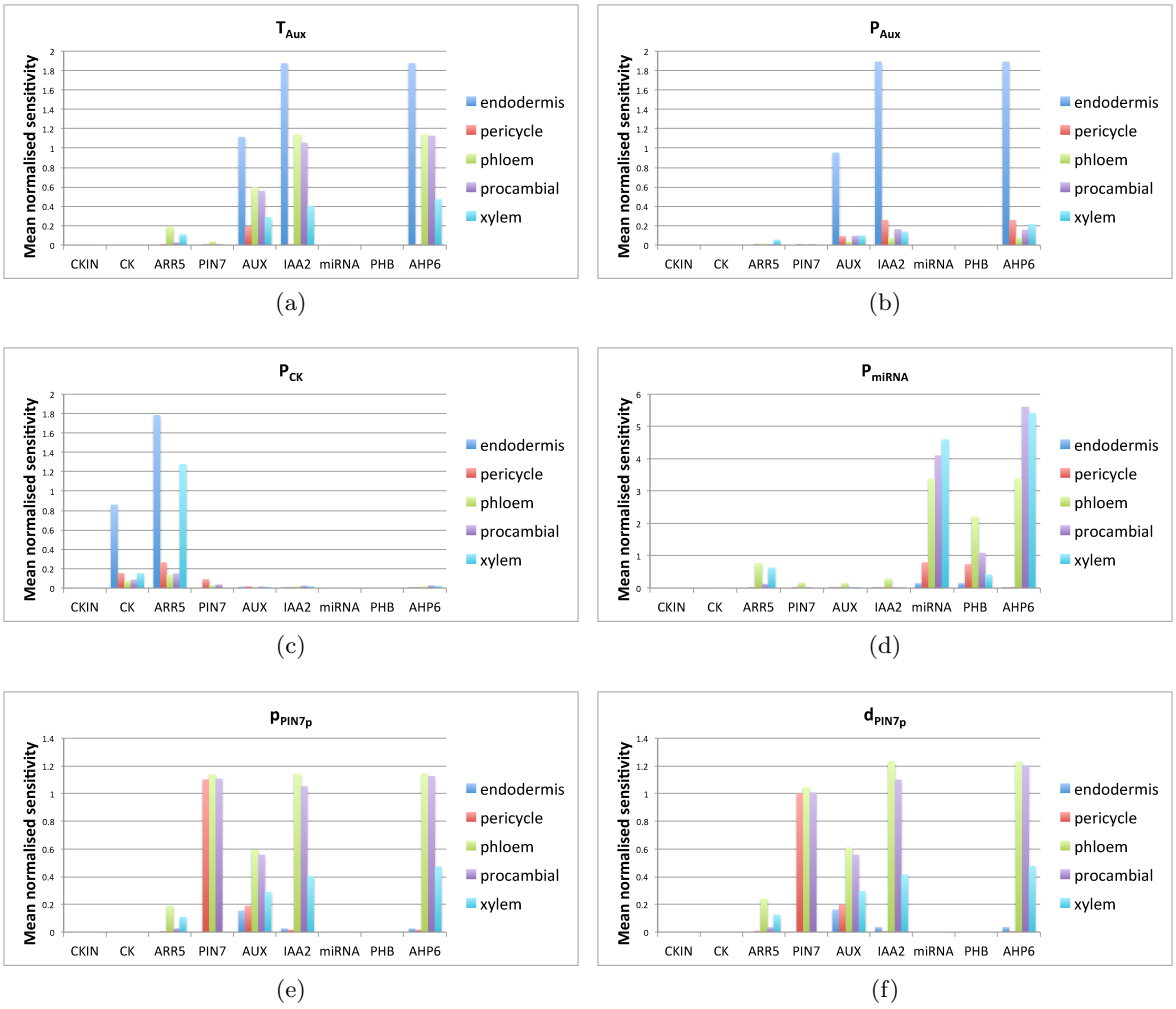

Figure 17: Series of plots representing the mean, calculated for all cells in a particular tissue and for all tissues, of the normalized sensitivity index given by Eq. (24). Parameters associated with the cell geometry (T_{Aux}, P_{Aux}, P_{CK}, P_{miRNA}, p_{PIN7_p}, d_{PIN7_p}) are perturbed 10% above their default value reported in Supplementary Tables 2, 3. T_{Aux}, P_{Aux} influence mainly the sensitivity of auxin, IAA2 and AHP6; P_{Ck} affects mainly cytokinin, ARR5 and PIN7; perturbations in P_{miRNA} act mostly on miRNA, PHB and AHP6.

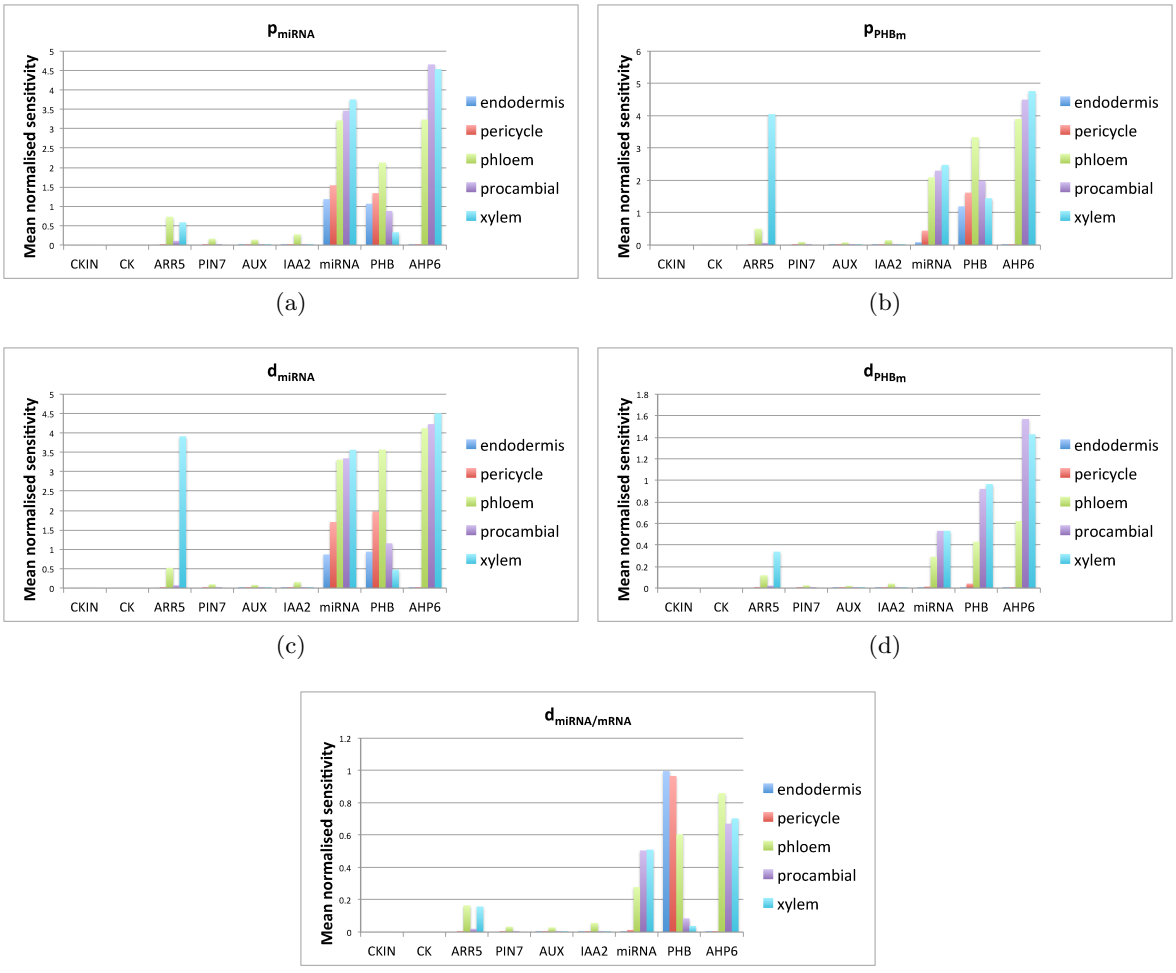

Figure 18: Series of plots representing the mean, calculated for all cells in a particular tissue and for all tissues, of the normalised sensitivity index given by Eq. (24). Parameters associated with PHB mRNA and miRNA165/6 (p_{miRNA}, p_{PHB_m}, d_{miRNA}, d_{PHB_m}, $d_{miRNA/mRNA}$) are perturbed 10% above their default value reported in Supplementary Tables 2, 3. Perturbations in these parameters affect mainly $miRNA$, PHB_p, $AHP6_p$, $ARR5_p$ in the tissues in which these components are present.

for $i = 1, 2$, where:

$$
\begin{aligned}
F^{(i)}_{AHP6_m} &= \frac{([Aux]_i/\theta_{Aux})^{m_{Aux}}}{1 + ([Aux]_i/\theta_{Aux})^{m_{Aux}} + (PHB/\theta_{PHB})^{m_{PHB}}}, \\
F^{(i)}_{ARR5_m} &= \frac{(Ck/\theta_{Ck})^{m_{Ck}}}{1 + (Ck/\theta_{Ck})^{m_{Ck}} + ([AHP6p]_i/\theta_{AHP6})^{m_{AHP6}}}, \\
F^{(i)}_{PIN7_m} &= \frac{([ARR5p]_i/\theta_{ARR5})^{m_{ARR5}}}{1 + ([ARR5p]_i/\theta_{ARR5})^{m_{ARR5}}}.
\end{aligned}
$$

Unless stated otherwise, all parameters and variables are as previously defined.

Figure 19 shows the steady states for *auxin*, $PIN7_m$, $AHP6_m$ and $ARR5_m$ in one of the cells for increasing values of p_{aux}, the auxin biosynthesis rate (the results are identical in both cells). At low p_{aux} there is a single steady state with low *AHP6* expression resulting in high *PIN7* expression in both cells so that the level of auxin is equal in both. At high p_{aux} there is also a single steady state in which the level of auxin is balanced in both cells, but here the high level of AHP6 strongly represses *ARR5* and so little or no *PIN7* is expressed in either cell. At intermediate values for p_{aux} there exist two additional stable steady states representing the cases where there there is asymmetry in expression between the two cells, with high ARR5 and PIN7 and low AHP6 and auxin in one cell, and vice versa in the other cell. These additional stable branches end with limit points, from which four unstable steady states double back and meet the symmetric steady state branch at two subcritical pitchfork bifurcations, themselves linked by one final unstable steady state. This final unstable steady state represents the range of values for p_{aux} for which gene expression is balanced between the two cells but in which any small perturbation from that steady state is likely to lead to a switch to the case with an asymmetry in gene expression.

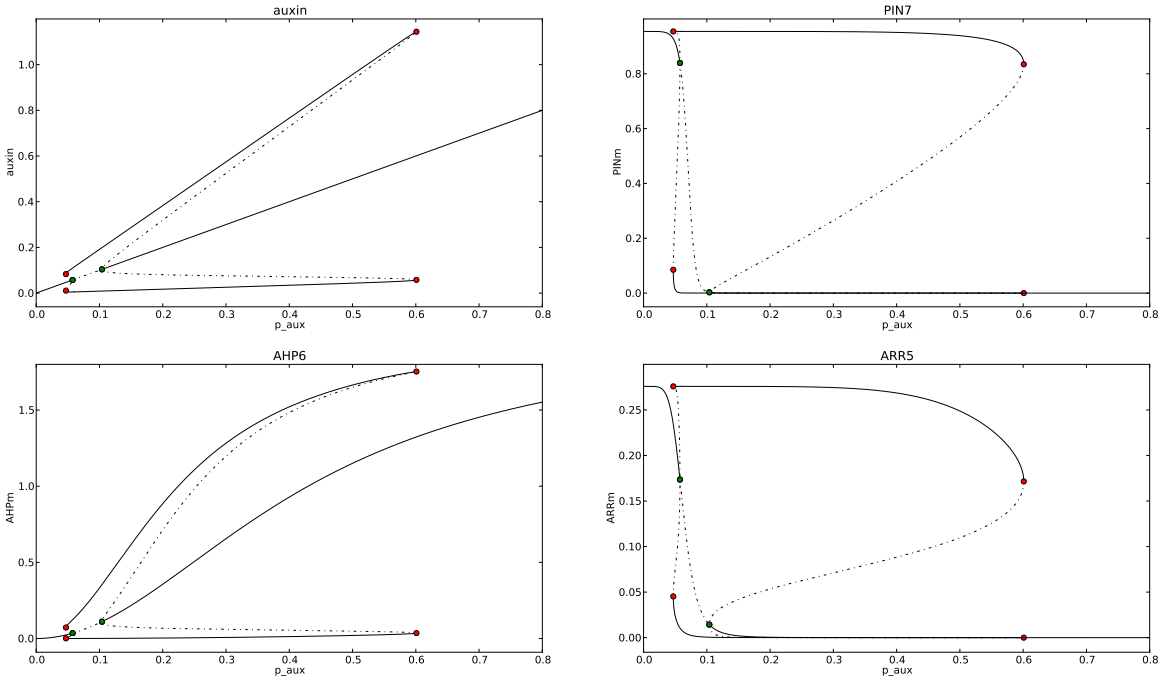

Figure 19: Steady states for *auxin*, $PIN7_m$, $AHP6_m$ and $ARR5_m$ (in either cell) for increasing values of the auxin production rate p_{aux} in the model given by equations (25). Red dots indicate limit points, green dots pitchfork bifurcations, solid lines stable steady states, dotted lines unstable steady states.

This result suggests that in the two cell case at least, once an imbalance in *PIN7* expression has been established between the two cells, there is relatively broad range of auxin production rates within which this imbalance is maintained, providing a hypothetical mechanism for maintaining a pattern. Furthermore, a range of auxin production also exists within which, even when expression is balanced between the two cells, the system is sensitive to small perturbations and will switch to the case where *PIN7* is strongly expressed in one cell only, providing a hypothetical mechanism for establishing a pattern.

Plotting the steady states for increasing levels of Ck and PHB results in similar, but not identical bifurcation structures as for p_{aux}. For PHB, there is no positive lower limit to the bistable region, so that below a threshold value of PHB the system is only stable with high PIN7 in one cell and low PIN7 in the other (Figure 20A). Above another threshold of PHB there exists only one stable steady state in which PIN7 is equal in both cells, and between the two thresholds there is a region in which the system may be stable in either a balanced or imbalanced state. Finally, as with *auxin*, for low and high Ck there is a single stable steady state where *PIN7* is respectively

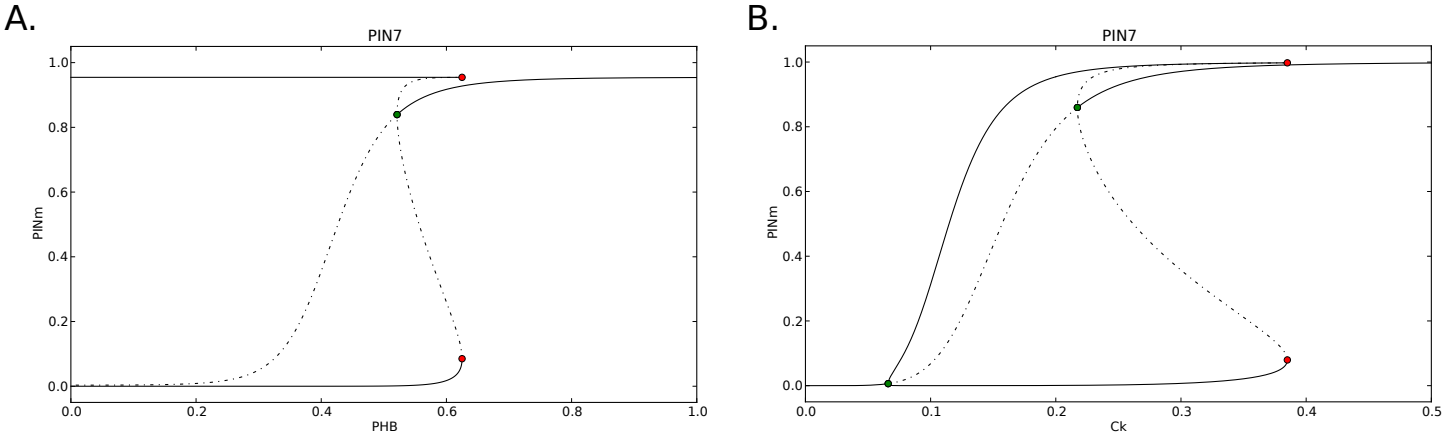

Figure 20: Steady states for $PIN7_m$ (in either cell) for increasing values of PHB (A.), and Ck (B.) in the model given by equations (25). Red dots indicate limit points, green dots pitchfork bifurcations, solid lines stable steady states, dotted lines unstable steady states.

expressed weakly and strongly in both cells, and for intermediate values multiple steady states are possible (Figure 20B). As with *auxin*, at the top end of this intermediate Ck range there are two limit points and a subcritical pitchfork bifurcation bounding a range in which *PIN7* may either be expressed stably equally in both cells, or strongly in one cell and weakly in the other. Unlike with *auxin* however, the lower bound of the bistable range occurs at a supercritical pitchfork bifurcation.

5 Mathematical model applied in Supplementary Movies 10-14

In this section, we extend the mathematical model developed in section 1 to include the regulatory effect of SHORT ROOT (SHR) on miRNA165/6. SHR is produced in the vascular cylinder and moves into the endodermis to bind SCARECROW (SCR) [22]. Once in the endodermis, the protein complex SHR-SCR promotes the transcription of *miRNA165/6* [12]. Endodermally produced *miRNA165/6* then degrades its target mRNA *PHB* in the endodermis and stele periphery. In our model, we assume that transcription and translation of *SHR* occurs in all tissues except for the endodermis:

$$\emptyset \xrightarrow{p_{SHR_m}} \mathrm{SHR}_m, \qquad \mathrm{SHR}_m \xrightarrow{d_{SHR_m}} \emptyset,$$

$$\mathrm{SHR}_m \xrightarrow{p_{SHR_p}} \mathrm{SHR}_m + \mathrm{SHR}_p, \qquad \mathrm{SHR}_p \xrightarrow{d_{SHR_p}} \emptyset.$$

SHR protein is allowed to diffuse and activates the expression of *miRNA165/6* in the endodermis. Although this activation would involve binding with SCR, we simplify this redundant process by assuming SHR to directly regulate miRNA165/6 transcription in the endodermis only. Transcription of miRNA165/6 is controlled by the Hill function:

$$F^{(i)}_{miRNA165/6}([\mathrm{SHR}]_i) = \frac{([\mathrm{SHR}]_i/\theta_{SHR})^{m_{SHR}}}{1+([\mathrm{SHR}]_i/\theta_{SHR})^{m_{SHR}}}, \tag{26}$$

As a result, *SHR* mRNA and protein levels are governed by the equations:

$$\begin{aligned}
\frac{d[\mathrm{SHR}_m]_i}{dt} &= \begin{cases} 0, & \text{if } i \text{ is in the endodermis,} \\ p_{SHR_m} - d_{SHR_m}[\mathrm{SHR}_m]_i, & \text{otherwise,} \end{cases} \\
\frac{d[\mathrm{SHR}_p]_i}{dt} &= p_{SHR_p} - d_{SHR_p}[\mathrm{SHR}_p]_i \\
&\quad - \frac{1}{V_i}\sum_{n\in N_i} S_{i,n} P_{SHR}\Big([\mathrm{SHR}_p]_i - [\mathrm{SHR}_p]_n\Big),
\end{aligned} \tag{27}$$

Parameter	Description	Value
p_{SHR_m}	*SHR* mRNA transcription rate	$1.0 \cdot \mu M \cdot s^{-1}$
d_{SHR_m}	*SHR* mRNA degradation rate	$1.0 \cdot s^{-1}$
θ_{SHR}	SHR binding threshold	$0.05 \cdot \mu M$
m_{SHR}	SHR Hill coefficient	2
P_{SHR}	SHR background permeability	$10.0 \cdot \mu m \cdot s^{-1}$
p_{SHR_p}	SHR protein translation rate	$1.0 \cdot s^{-1}$
d_{SHR_p}	SHR protein degradation rate	$1.0 \cdot s^{-1}$

Table 11: *Default values of the parameters applied in Supplementary Movies 10-14 together with the default parameters in Supplementary Tables 2 and 3.*

whereas the equation for miRNA165/166 takes the form:

$$\begin{aligned}\frac{d[\text{miRNA165/166}]_i}{dt} &= p_{miRNA} F^{(i)}_{miRNA165/6} - d_{miRNA}[\text{miRNA165/166}]_i \\ &\quad - d_{miRNA/mRNA}[\text{PHB}_m]_i[\text{miRNA165/166}]_i \\ &\quad - \frac{1}{V_i}\sum_{n\in N_i} S_{i,n} P_{miRNA}\Big([\text{miRNA165/166}]_i - [\text{miRNA165/166}]_n\Big), \end{aligned} \tag{28}$$

where i is the cell index. In agreement with experimental observations on *PIN7* expression (see Figure 4), in Supplementary Movie 12 all vascular cells are allowed the potential to express *PIN7* . The extended model is then defined by Eqs. (1)-(28) substituting Eq. (28) to the equation for miRNA165/6 transcription in Eqs. (6). The default parameter values of the extended model are defined in Supplementary Table 11 together with the ones reported in Supplementary Tables 2 and 3.

6 Plant Lines

All plant lines were in the Columbia background. the *TCSn::GFP* line was provided by Bruno Müller [24]. The *ARR5::GUS* line was published in [25], *PIN1::PIN1::GFP*, *PIN3::PIN3:GFP* and *PIN7::PIN7:GFP* were published in [26, 27], *DR5rev::GFP* was published in [28], *AHP6::GFP* in [23], *PHB::PHB:GFP* in [29], *AUX1::AUX1:GFP* in [30] and *IAA2::GUS* in [3].

References

[1] Friml J et al. (2002) Lateral relocation of auxin efflux regulator PIN3 mediates tropism in Arabidopsis. Nature 14:806-809.

[2] Blilou I et al. (2005) The PIN auxin efflux facilitator network controls growth and patterning in Arabidopsis roots. Nature 433:39-44.

[3] Bishopp A et al. (2011) A mutually inhibitory interaction between auxin and cytokinin specifies vascular pattern in roots. Curr Biol. 21:917-26.

[4] Pound MP et al. (2012) CellSeT: Novel Software to Extract and Analyze Structured Networks of Plant Cells from Confocal Images. Plant Cell 24:1353-1361.

[5] Pradal C, Boudon F, Nouguier C, Chopard J & Godin C (2009). PlantGL: a Python-based geometric library for 3D plant modelling at different scales. Graphical Models. 71:1-21.

[6] Levine E, McHale P & Levine H (2007) Small regulatory RNAs may sharpen spatial expression patterns. PLoS Comput Biol. 2007 3:e233.

[7] Stoma S et al. (2008) Flux-Based Transport Enhancement as a Plausible Unifying Mechanism for Auxin Transport in Meristem Development. PLoS Comput Biol. 4:e1000207.

[8] Liu J et al. (2010) Modelling and experimental analysis of hormonal crosstalk in Arabidopsis. Mol Sys Biol. 6:373.

[9] Rausenberger J et al. (2011) Photoconversion and Nuclear Trafficking Cycles Determine Phytochrome A's Response Profile to Far-Red Light. Cell 146:813-825.

[10] Laskowski M et al. (2008) Root System Architecture from Coupling Cell Shape to Auxin Transport. PLoS Biol 6: e307.

[11] Grieneisen VA, Xu J, Mare AFM, Hogeweg P & Scheres B (2007) Auxin transport is sufficient to generate a maximum and gradient guiding root growth. Nature 449:1008-1013.

[12] Carlsbecker A et al. (2010) Cell signaling by microRNA165/6 directs gene dose-dependent root cell fate. Nature 465: 316-321.

[13] Alves F & Dilão R (2006) Modeling segmental patterning in Drosophila: Maternal and gap genes. J Theor Biol, 241 342-359.

[14] Zheng Y et al. (2006) Comparative study of parameter sensitivity analyses of the TCR-activated Erk-MAPK signalling pathway. Syst Biol (Stevenage) 153(4):201-11.

[15] Schmidt H & Jirstrand M (2006) Systems Biology Toolbox for MATLAB: A computational platform for research in Systems Biology. Bioinformatics. 22:514-515.
[16] Varma A, Morbidelli M & Wu H (1999) Parametric Sensitivity in Chemical Systems. Cambridge University Press, New York.
[17] Saltelli A, et al. (1999) A Quantitative Model-Independent Method for Global Sensitivity Analysis of Model Output. Technometrics 41, (1), pp. 39-56.
[18] Beguerisse-Diaz M et al. (2012) Compound stress response in stomatal closure: a mathematical model of ABA and ethylene interaction in guard cells. BMC Systems Biology 6:146.
[19] Marino S et al. (2008) A methodology for performing global uncertainty and sensitivity analysis in systems biology. J Theor Biol. 254(1):178-96.
[20] Sourjik V et al. (2002) Binding of the Escherichia coli response regulator CheY to its target measured in vivo by fluorescence resonance energy transfer. Proc Natl Acad Sci U S A 99: 12669-12674.
[21] Edelstein SJ et al. (2010) Ligand Depletion in vivo Modulates the Dynamic Range and Cooperativity of Signal Transduction. PLoS ONE 5(1): e8449.
[22] Cui et al (2007) An evolutionarily conserved mechanism delimiting SHR movement defines a single layer of endodermis in plants. Science 316:421-425.
[23] Mahonen et al (2006) Cytokinin signaling and its inhibitor AHP6 regulate cell fate during vascular development. Science 311:94-8.
[24] Zürcher et al. (2013) A robust and sensitive synthetic sensor to monitor the transcriptional output of the cytokinin signaling network in planta. Plant Physiol. 161:1066-1075.
[25] D'Agostino IB, Deruere J & Kieber JJ (2000) Characterization of the response of the Arabidopsis response regulator gene family to cytokinin. Plant Physiol 124: 1706-1717.
[26] Benkova E et al. (2003) Local, efflux-dependent auxin gradients as a common module for plant organ formation. Cell 115: 591-602.
[27] Blilou I et al. (2005) The PIN auxin efflux facilitator network controls growth and patterning in Arabidopsis roots. *Nature* 433:39-44.
[28] Friml J et al. (2003). Efflux-dependent auxin gradients establish the apical-basal axis of Arabidopsis. Nature 426: 147-153.
[29] Miyashima S, Koi S, Hashimoto T & Nakajima K (2011) Non-cell-autonomous microRNA165 acts in a dose-dependent manner to regulate multiple differentiation status in the Arabidopsis root. Development 138: 2303-2313.
[30] Swarup R et al. (2004) Structure and function of the presumptive Arabidopsis auxin permease AUX1. Plant Cell 16:3069-3083.